

JULIUS-MAXIMILIANS-UNIVERSITÄT WÜRZBURG



FAKULTÄT FÜR PHYSIK UND ASTRONOMIE  
LEHRSTUHL FÜR THEORETISCHE PHYSIK II

MASTERARBEIT

---

THE COMBINATION OF  $\mu \rightarrow 3e$  AND NEUTRINO  
PHENOMENOLOGY AS A PROBE FOR A  
LEFT-RIGHT-SYMMETRIC MODEL

---

Matthias Kübert  
vorgelegt am:  
7. Oktober 2016  
Betreuer: Prof. Dr. Werner Porod



## Zusammenfassung

Ziel dieser Arbeit war es mithilfe von Neutrinophysik, Einschränkungen für Yukawakopplungen in einem Links-Rechts Symmetrischen Modell zu finden. Im Laufe dessen wurde in der seltene Lepton Zerfall  $\mu^- \rightarrow e^- e^+ e^-$  berechnet. In diesem Modell hat dieser Zerfall *tree-level* Beiträge, die im Standard Modell verboten sind, da sie einen Flavour-Changing Neutral-Current darstellen. Um den Zerfall vollständig zu berechnen wurde zuerst ein kompliziertes Phasenraum Integral bestimmt, welches unter der Näherung verschwindender Elektronenmasse, ausgewertet wurde. Als die Zerfallsbreite, sowie das Verzweigungsverhältnis berechnet waren wurden Neutrinodaten benutzt um die Anzahl der Parameter von denen das Verzweigungsverhältnis abhängig ist reduziert. Hierfür wurde der See-Saw Mechanismus herangezogen. Es ergaben sich hierfür aufgrund quadratischer Gleichungen, mehrere gültige Lösungen. Am Ende blieb ein Ausdruck für das Verzweigungsverhältnis stehen, der nur noch von drei Diagonaleinträgen einer Bidublett Yukawakopplung, sowie  $\tan \beta$  abhängt und vier Lösungen hat. Für diese vier Lösungen wurden Datensätze berechnet und es wurde mit Hilfe experimenteller Zwangsbedingungen abgeschätzt welcher Bereich des Parameterraums vom Experiment aus- oder eingeschlossen ist.



## Abstract

The goal of this thesis was to find means to link neutrino physics with rare lepton decays, in order to find constraints for Yukawa couplings in a Left-right-symmetric model. Therefore, the decay  $\mu^- \rightarrow e^- e^+ e^-$  was computed. In this model, it is realised at tree level, which is not allowed in the SM, as this would be a FCNC. In order to compute the decay width and branching ratio, a rather complicated phase space integration needed to be evaluated. This integral was computed in the limit of vanishing electron masses, as it would otherwise lead to a highly complicated integration. Afterwards, the see-saw mechanism was used to constrain the Yukawa couplings and in the end, the final form for the branching ratio was only dependant on three diagonal entries of a bidoublet Yukawa coupling and  $\tan\beta$ . Additionally, it turned out that quadratic equations led to four different solutions of the branching ratio. These have been used to compute datasets for the branching ratio and experimental bounds have been used to find out which regions have been ruled out by the experiment and which regions were not.



# Contents

<b>1. Introduction</b>	<b>1</b>
<b>2. Neutrino Physics</b>	<b>3</b>
2.1. Neutrino Oscillation . . . . .	3
2.2. See-Saw Mechanism . . . . .	5
<b>3. LRM</b>	<b>7</b>
<b>4. Calculating The Decay</b>	<b>11</b>
4.1. Transition Amplitudes . . . . .	11
4.2. Rewriting The Traces . . . . .	16
4.3. Phase Space Integration . . . . .	18
4.4. Evaluating Integrals . . . . .	27
<b>5. Connection To Neutrino Physics</b>	<b>31</b>
<b>6. Discussion</b>	<b>35</b>
6.1. First Solution . . . . .	35
6.2. Second Solution . . . . .	40
6.3. Third Solution . . . . .	46
6.4. Fourth Solution . . . . .	46
6.5. $\tan \beta = 1$ . . . . .	53
<b>7. Summary</b>	<b>55</b>
<b>A. Appendix</b>	<b>57</b>
A.1. Model Parameters . . . . .	57
A.2. Readout Parameter Range . . . . .	58
A.3. Additional Plots . . . . .	62
<b>Bibliography</b>	<b>67</b>
<b>Eigenständigkeitserklärung</b>	<b>68</b>



# 1. Introduction

The neutrino has always been highly elusive - both in its nature and its theoretical concept - to the extent that back when Wolfgang Pauli proposed it in 1930, he even felt the need to apologize for it, with the words: "*I have done a terrible thing, I have postulated a particle that cannot be detected.*" [14] Since then, many discoveries about its nature have been made, but at the same time more questions have been raised than answered. We know now, that the solar models for neutrino emission are in fact correct as solar neutrinos did not vanish on their way to earth. They simply changed their flavour. Together with the same discovery for atmospheric neutrinos, the concept of neutrino oscillation which proved that - contrary to standard model (SM) assumptions - neutrinos indeed have a non-zero mass, was developed. For this discovery the Nobel Prize in Physics was awarded to Takaaki Kajita and Arthur B. McDonald in 2015 [15, 7].

So far, working this newly gained knowledge into the standard model has not led to an overhauled, self-consistent theory beyond the standard model (BSM), supported by experiments. Various loose ends remain that the current state of research simply cannot yet tie up. Apart from some steps in the right direction, like measurements of the mixing angles in the so-called *PMNS*-matrix for example, major questions still require research. The nature of the masses - Dirac or Majorana - as well as the hierarchy of the mass spectrum or the status of lepton CP symmetry, to mention only a few, are still unknown. An pathway for BSM physics lies in the chirality of SM neutrinos.

Standard model neutrinos are realized in left-handed leptonic  $SU(2)_L$  doublets. A scenario to generate masses within the so-called see-saw mechanism proposes a right-handed heavy partner for the SM neutrino. Incidentally, the right-handed charged leptons can be realised in  $SU(2)_R$  doublet, as opposed to singlets in the SM. Unfortunately, the scale at which it takes place, is the the scale of grand unified theories (GUT) at roughly  $10^{15}$  GeV, barring it from direct experimental testing with current devices [7]. But that does not imply that current means of research are incapable of producing further insight. There is in fact another way to tackle the subject of neutrino masses and that is rare lepton decay. In the course of this thesis the Left-Right symmetric model (*LRM*), a model that allows massive right handed neutrinos will be used to compute the tree level amplitude of the  $\mu \rightarrow e^-e^-e^+$  decay, for which the SM only provides loop level decays. As Yukawa couplings for charged leptons are the same as for neutrinos, when inserted into the formula for the decay, data from neutrino physics can be used to constrain the parameters of the model [2].

Hence, the goal of this thesis is to find a means to combine neutrino data with the  $\mu \rightarrow 3e$  decay in order to find constraints for the Yukawas. Chapter 2 will provide a brief introduction to neutrino oscillation and the see-saw mechanism. The following chapter will briefly explain the foundations of the LRM, which are crucial to the understanding of the computation of tree level decay in Chapter 4. In Chapter 5, the neutrino data will

## *1. Introduction*

---

be rewritten and inserted into the rare muon decay. Finally, that form will be used to compute plots as functions of several input parameters, to determine whether the configuration of these parameters produces a branching ratio supported by the experimental bounds.

## 2. Neutrino Physics

Several pioneering discoveries concerning neutrinos have been made in the recent past, giving insight into BSM physics, to which this chapter seeks to give a brief introduction (for more Information, see Ref. [15]).

### 2.1. Neutrino Oscillation

As they are leptons, neutrinos appear in three different generations, just as their charged leptonic counterparts, which are called flavour states  $|\nu_\alpha\rangle$  (with  $\alpha = e, \mu, \tau$ ). However, these are different from their mass eigenstates  $|\nu_i\rangle$  (with  $i = 1, 2, 3$ ) as they are transformed by a unitary Matrix  $U$  in the following way:

$$|\nu_i\rangle = U_{i\alpha} |\nu_\alpha\rangle \quad \text{and} \quad |\nu_\alpha\rangle = U_{\alpha i}^{-1} |\nu_i\rangle \quad (2.1)$$

$U$  is also known as the *Pontecorvo-Maki-Nakagawa-Sakata* matrix or in short *PMNS* matrix. Note that both flavour and mass eigenstates are assumed to form a basis. In order to obtain the vacuum transition amplitude, the time evolution will be applied to the mass states:

$$|\nu_k(t)\rangle = \exp(-iE_k \cdot t) |\nu_k\rangle \quad (2.2)$$

together with the unitarity of  $U$  and eq. (2.1) yields

$$\begin{aligned} A_{\nu_\alpha \rightarrow \nu_\beta} &:= A_{\alpha\beta} = \langle \nu_\beta | \nu_\alpha(t) \rangle \\ &= \sum_{k=1}^3 U_{\alpha k}^* U_{\beta k} \exp(-iE_k \cdot t). \end{aligned} \quad (2.3)$$

Therefore, the transition probability  $P_{\alpha\beta}$  is

$$P_{\alpha\beta} = A_{\alpha\beta}^* \cdot A_{\alpha\beta} = \sum_{k,j} U_{\alpha k}^* \underbrace{U_{\beta k} U_{\alpha j} U_{\beta j}^*}_{:= J_{kj}^{\alpha\beta}} \exp(-i(E_k - E_j) \cdot t) \quad (2.4)$$

In the reasonable limit of ultra-relativistic neutrinos ( $m_\nu = \mathcal{O}(eV)$ ),  $E_k$  yields

$$E_k = \sqrt{\vec{p}^2 + m_k^2} \approx E + \frac{m_k^2}{2E}. \quad (2.5)$$

Which in turn inserted into eq. (2.4) becomes

$$P_{\alpha\beta} = \delta_{\alpha\beta} - \underbrace{4 \sum_{k>j} \text{Re} J_{kj}^{\alpha\beta} \sin^2 \left( \frac{\Delta m_{kj}^2 L}{4E} \right)}_{\text{CP conserving}} + \underbrace{2 \sum_{k>j} \text{Im} J_{kj}^{\alpha\beta} \sin^2 \left( \frac{\Delta m_{kj}^2 L}{2E} \right)}_{\text{CP violating}}$$

wherein  $L$  is the distance between detector and source, commonly referred to as *baseline*,  $\Delta m_{kj}^2 = m_k^2 - m_j^2$  the squared difference between two mass eigenstates and  $\delta_{\alpha\beta}$  is the Kronecker delta. Note that the first braced term is  $CP$  conserving whereas the second braced term violates  $CP$ . It is important to understand that the observed oscillation only depends on the differences of the squared masses, implying that it is impossible to determine both the *offset* and the *hierarchy* of the mass spectrum via oscillation. There are two hierarchies, called *normal* hierarchy if  $m_1 < m_2 < m_3$ , and *inverted* if  $m_3 < m_1 < m_2$ .

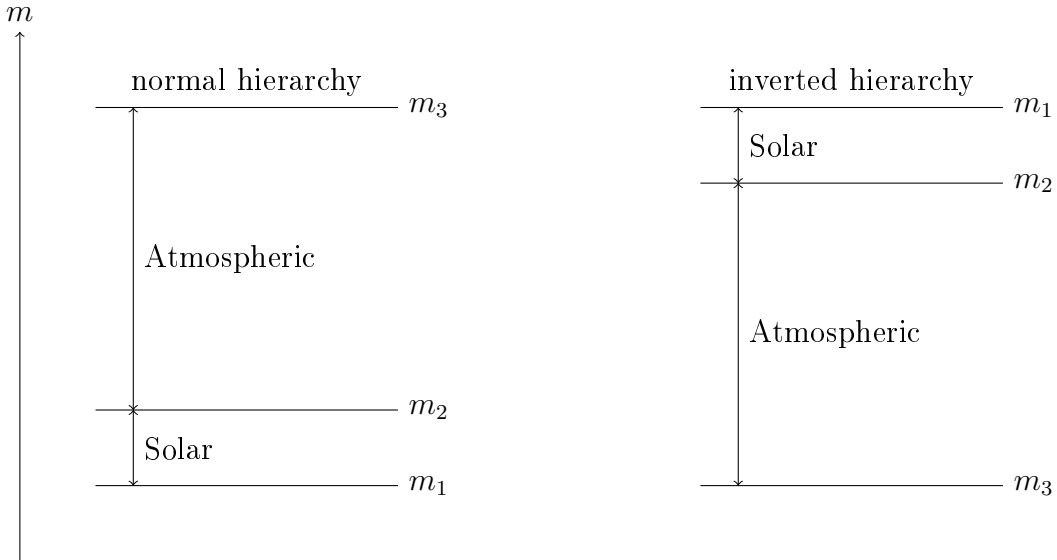


Figure 2.1.. Schematic neutrino mass eigenstates for both hierarchies.

The mixing matrix can be parametrized as

$$U_{PMNS} = \underbrace{\begin{pmatrix} 1 & 0 & 0 \\ 0 & c_{23} & s_{23} \\ 0 & -s_{23} & c_{23} \end{pmatrix}}_{\text{Atmospheric mixing}} \cdot \underbrace{\begin{pmatrix} c_{13} & 0 & s_{13}e^{-\delta_{cp}} \\ 0 & 1 & 0 \\ -s_{13}e^{-\delta_{cp}} & 0 & c_{13} \end{pmatrix}}_{\text{Reactor mixing}} \cdot \underbrace{\begin{pmatrix} c_{12} & s_{12} & 0 \\ -s_{12} & c_{12} & 0 \\ 0 & 0 & 1 \end{pmatrix}}_{\text{Solar mixing}} \cdot \begin{pmatrix} 1 & 0 & 0 \\ 0 & \exp^{i\frac{\alpha_{21}}{2}} & 0 \\ 0 & 0 & \exp^{i\frac{\alpha_{31}}{2}} \end{pmatrix} \quad (2.6)$$

with  $s_{ij} = \sin \theta_{ij}$ ,  $c_{ij} = \cos \theta_{ij}$  and  $\delta_{CP}$  as a  $CP$  phase and  $\alpha_{21}$  and  $\alpha_{31}$  are Majorana phases. The names atmospheric for  $\theta_{23}$ , reactor for  $\theta_{13}$  and solar mixing angle for  $\theta_{12}$

have historic reasons. Current results for the mixing angles and  $\Delta m^2$  are given in table 2.1

Parameter	Best-fit value
$\Delta m_{21}^2$	$(7.53 \pm 0.18) \cdot 10^{-5} \text{eV}^2$
$\Delta m_{32}^2$	$(2.44 \pm 0.06) \cdot 10^{-3} \text{eV}^2$
$\sin^2(\theta_{12})$	$0.304 \pm 0.014$
$\sin^2(\theta_{23})$	$0.514_{-0.056}^{+0.055}$
$\sin^2(\theta_{13})$	$(2.19 \pm 0.12) \cdot 10^{-2}$

Table 2.1.. Experimental best-fit values for neutrino oscillation data in a normal hierarchy. Data taken from Ref [9].

## 2.2. See-Saw Mechanism

Experimentally, not much is known about neutrino masses, yet there is a concept to explain the mass generation in theory. There are two distinct classes of masses, allowed in an electroweak Lagrangian and that is either Dirac or Majorana [1]. A Dirac mass term is of the form

$$\mathcal{L}_D = -m_D (\bar{\nu}_L N_R + \bar{N}_R \nu_L), \quad (2.7)$$

and a Majorana mass term is of this form:

$$\mathcal{L}_M = -\frac{1}{2} m_M^L (\bar{\nu}_L \nu_L^c + \bar{\nu}_L^c \nu_L) - \frac{1}{2} m_M^R (\bar{N}_R N_R^c + \bar{N}_R^c N_R). \quad (2.8)$$

It is now possible to express the neutrino fields in a left handed vector  $n_L$  like this:

$$n_L = \begin{pmatrix} \nu_L \\ N_R^c \end{pmatrix}, \quad \text{and} \quad \bar{n}_L^c = (\bar{\nu}_L^c \quad \bar{N}_R) \quad (2.9)$$

With this definition, the mass matrix  $M$  can be introduced.

$$\mathcal{L}_{M+D} = \mathcal{L}_M + \mathcal{L}_D = -\frac{1}{2} \bar{n}_L^c M n_L + \text{h.c.}, \quad (2.10)$$

with

$$M = \begin{pmatrix} m_L & m_D \\ m_D^T & m_R \end{pmatrix}. \quad (2.11)$$

This matrix has two positive mass eigenstates:

$$m_{1,2} = \left| \frac{1}{2} \left( m_L + m_R \pm \sqrt{(m_L - m_R)^2 + 4m_D^2} \right) \right|. \quad (2.12)$$

The see-saw mechanism is based on the notion that the right handed neutrino field  $N_R$  is of a heavy mass. However,  $m_D$  is of the electroweak scale and thus  $m_D \ll m_R$ . Furthermore,  $\nu_L$  possesses non-zero isospin and hypercharge which is why the left handed Majorana term is forbidden by SM gauge symmetries. So, as a consequence  $m_L = 0$ . Which is why the eigenstates are

$$\begin{aligned} m_1 &\approx \frac{m_D^2}{m_R} \\ m_2 &\approx m_R \end{aligned}$$

(see also Ref. [1]). Thus, the right handed neutrino has to be at a mass scale where new physics kicks in  $\Lambda_{BSM} = m_R$  and the mass of the very light neutrino is thus highly suppressed with  $m_D/\Lambda_{BSM}$ . In fact, in order to satisfy experimental bounds for neutrino masses,  $\Lambda_{BSM}$  has to be close to the GUT scale. This also explains the name *see-saw*: The heavy right handed particle pushes the light left-handed mass up, like in a real see-saw [6, 7, 3].

### 3. LRM

Left right symmetric extensions of the SM feature this gauge group

$$SU(3)_C \times SU(2)_L \times SU(2)_R \times U(1)_{B-L} \quad (3.1)$$

(see also Ref. [2, 3]). Note, that in this gauge group the charge of the  $U(1)$  group is not the unphysical  $Y$  hypercharge, as in the SM, but  $B - L$ . That is: Baryon number  $B$  minus lepton number  $L$ . Incidentally, contrary to the SM charge, this is an actual physical quantity. The electric charge  $Q$  can be obtained by:

$$Q = T_{3_L} + T_{3_R} + \frac{B - L}{2} \quad (3.2)$$

In the following discussion, only the leptonic part of the Lagrangian will be examined

$$\mathcal{L}_{LRM,L} = Y_1 \bar{L}_L \phi L_R + Y_2 \bar{L}_L \tilde{\phi} L_R + \frac{1}{2} Y_L \bar{L}_L \Delta_L L_L^c + \frac{1}{2} Y_R \bar{L}_R^c \Delta_R L_R + \text{h.c.} \quad (3.3)$$

with leptonic  $SU(2)$  doublets:

$$L_L = \begin{pmatrix} \nu_L \\ l_L \end{pmatrix} \sim (1, 2, 1, -1); L_R = \begin{pmatrix} N_R \\ l_R \end{pmatrix} \sim (1, 1, 2, -1) \quad (3.4)$$

Note, that both  $L_L$  and  $L_R$  hold for all three generations  $e, \mu$  and  $\tau$ , but - for the sake of simplicity - only one generation will be assumed. The corresponding charges according to the gauge groups in eq. (3.1) are given in brackets. Furthermore  $Y_1, Y_2, Y_L, Y_R$  denote Yukawa couplings. Generally, these are  $3 \times 3$  matrices, but in the simplified case with only one flavour, which will be examined, these are scalars.  $\phi$  is a Higgs bidoublet and  $\tilde{\phi} = i\tau_2 \phi i\tau_2$  and  $\Delta_L, \Delta_R$  denote Higgs triplets.

The following definitions are according to Ref. [3]. The triplet  $\Delta_R$

$$\Delta_R = \begin{pmatrix} \delta_R^+/\sqrt{2} & \delta_R^{++} \\ \delta_R^0 & -\delta_R^+/\sqrt{2} \end{pmatrix} \sim (1, 1, 3, 2) \quad (3.5)$$

### 3. LRM

---

acquires a vacuum expectation value (VEV)

$$\langle \Delta_R \rangle = \begin{pmatrix} 0 & 0 \\ \frac{v_R}{\sqrt{2}} & 0 \end{pmatrix}, \quad (3.6)$$

breaking  $SU(2)_R \times U(1)_{B-L} \rightarrow U(1)_Y$ . This can only be achieved with  $v_R$  much greater than the scale of the electroweak symmetry breaking. The  $SU(2)_L$  triplet is:

$$\Delta_L = \begin{pmatrix} \delta_L^-/\sqrt{2} & \delta_L^{--} \\ \delta_L^0 & -\delta_L^-/\sqrt{2} \end{pmatrix} \sim (1, 3, 1, 2), \quad (3.7)$$

which also acquires a VEV

$$\langle \Delta_L \rangle = \begin{pmatrix} 0 & 0 \\ \frac{v_L}{\sqrt{2}} & 0 \end{pmatrix}. \quad (3.8)$$

The VEV  $v_L$  should be reasonably small in order to allow left handed neutrino masses of  $\mathcal{O}(\text{eV})$ .

The Higgs bidoublet  $\phi$  is for both  $SU(2)$  groups:

$$\phi = \begin{pmatrix} \phi_1^0 & \phi_2^+ \\ \phi_1^- & \phi_2^0 \end{pmatrix} \sim (1, 2, 2, 0), \quad (3.9)$$

The numbers in brackets denote the charges with the corresponding gauge groups according to eq. (3.1). Additionally it acquires a vacuum expectation value

$$\langle \phi \rangle = \begin{pmatrix} \frac{v_2}{\sqrt{2}} & 0 \\ 0 & \frac{v_1}{\sqrt{2}} \end{pmatrix} \quad (3.10)$$

at the scale  $v = \sqrt{v_2^2 + \kappa_1^2} = 174\text{GeV}$  (see Ref. [2]). Together with the first step of symmetry breaking, this results in the breaking of

$$\Rightarrow SU(2)_L \times SU(2)_R \times U(1)_{B-L} \rightarrow U(1)_Q. \quad (3.11)$$

If we now return to the Lagrangian of eq. (3.3) and only consider the neutrino part of it, namely

$$\mathcal{L}_{\nu, N} = Y_1 \bar{\nu}_L \phi N_R + Y_2 \bar{\nu}_L \tilde{\phi} N_R + \frac{1}{2} Y_L \bar{\nu}_L \Delta_L \nu_L^c + \frac{1}{2} Y_R \bar{N}_R^c \Delta_R N_R + \text{h.c.}, \quad (3.12)$$

and apply the symmetry breaking scheme from above,

$$\begin{aligned} \Rightarrow \mathcal{L}_{SB} &= \frac{1}{\sqrt{2}} Y_1 \bar{\nu}_L v_2 N_R + \frac{1}{\sqrt{2}} Y_2 \bar{\nu}_L v_1 N_R + \frac{1}{2} Y_L \bar{\nu}_L^c \frac{v_L}{\sqrt{2}} \nu_L + \frac{1}{2} Y_R \bar{N}_R^c \frac{v_R}{\sqrt{2}} N_R + \text{h.c.} \\ &= \frac{1}{\sqrt{2}} (Y_1 v_2 + Y_2 v_1) \bar{\nu}_L N_R + \frac{1}{2\sqrt{2}} Y_L v_L \bar{\nu}_L^c \nu_L + \frac{1}{2\sqrt{2}} Y_R v_R \bar{N}_R^c N_R + \text{h.c.}, \end{aligned} \quad (3.13)$$

---

this yields a mass matrix like in eq. (2.10)

$$\Rightarrow \widehat{M} = \begin{pmatrix} \sqrt{2}v_L Y_L & \frac{1}{\sqrt{2}}(Y_1 v_2 + Y_2 v_1) \\ \frac{1}{\sqrt{2}}(Y_1 v_2 + Y_2 v_1) & \sqrt{2}v_R Y_R \end{pmatrix}. \quad (3.14)$$

Thus, the Dirac masses in the LRM are:

$$m_D = \frac{1}{\sqrt{2}}(v_2 Y_1 + v_1 Y_2). \quad (3.15)$$

Therefore, the masses for the charged leptonic counterparts are:

$$M_L = \frac{1}{\sqrt{2}}(v_1 Y_1 + v_2 Y_2), \quad (3.16)$$

resulting in a form of the neutrino masses in the form of

$$m_\nu = m_L - m_D(m_R)^{-1}m_D^T, \quad (3.17)$$

which will be used later in Chapter 5 and is commonly referred to as the see-saw formula [2].



# 4. Calculating The Decay

## 4.1. Transition Amplitudes

The rare decay of  $\mu^- \rightarrow e^- e^- e^+$  is only feasible in the SM on loop level, as a tree level decay would be a FCNC [4]. In the LRM, however, the decay is possible at tree level. In order to obtain the tree level decay width, the amplitudes for the decay have to be calculated. In a first step, consider the full Lagrangian.

$$\begin{aligned} \mathcal{L} &= Y_1 \bar{L} P_R \phi L + Y_1^\dagger \bar{L} P_L \phi^\dagger L + Y_2 \bar{L} P_R \tilde{\phi} L + Y_2^\dagger \bar{L} P_L \tilde{\phi}^\dagger L + \frac{1}{2} Y_L \bar{L} P_R \Delta_L L^c + \frac{1}{2} Y_L^\dagger \bar{L}^c P_L \Delta_L^\dagger L \\ &\quad + \frac{1}{2} Y_R \bar{L}^c P_R \Delta_R L + \frac{1}{2} Y_R^\dagger \bar{L} P_L \Delta_R^\dagger L^c \\ &\Rightarrow \frac{1}{2} Y_R \underbrace{\bar{L}^c P_R \Delta_R L}_{L^T C P_R \Delta_R L} + \frac{1}{2} Y_L^\dagger \underbrace{\bar{L}^c P_L \Delta_L L}_{L^T C P_L \Delta_L^\dagger L} \end{aligned}$$

The Leptonic fields  $L$  and  $\bar{L}$  are of this form (see Ref. [11]):

$$\begin{aligned} L &= \int \frac{d^3 p}{(2\pi)^3 \sqrt{2E(p)}} \sum_{\mathbf{s}} (a_p^{\mathbf{s}} u^{\mathbf{s}}(p) e^{-ipx} + a_p^{\mathbf{s}c\dagger} v^{\mathbf{s}}(p) e^{ipx}) \\ \bar{L} &= \int \frac{d^3 p}{(2\pi)^3 \sqrt{2E(p)}} \sum_{\mathbf{s}} (a_p^\dagger \bar{u}^{\mathbf{s}}(p) e^{ipx} + a_p^{c\mathbf{s}} \bar{v}^{\mathbf{s}}(p) e^{-ipx}). \end{aligned}$$

Considering these two possible Feynman diagrams for the decay. The left diagram in figure 4.1 involves a neutral Higgs particle, whereas the right one involves a doubly charged Higgs scalar.

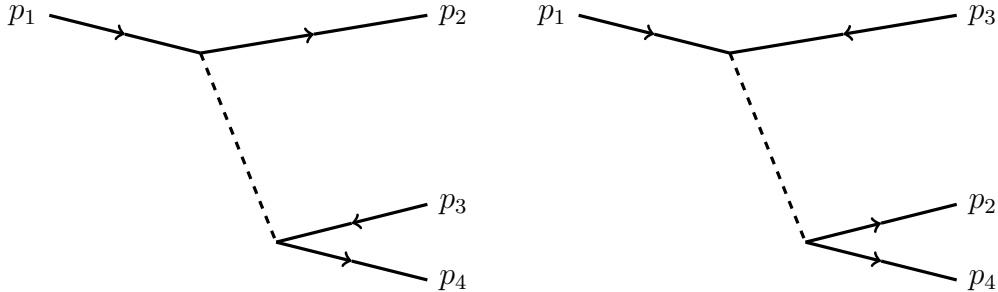


Figure 4.1.. left: neutral decay channel  $\Rightarrow \mathcal{M}_1$  right: doubly charged decay channel  $\Rightarrow \mathcal{M}_2$ .

In order to calculate the amplitudes for these decays, consider

#### 4. Calculating The Decay

---

$$\mathcal{M}_1 \Rightarrow \langle 0 | a(p_2) a^c(p_3) a(p_4) T \int dx (Y_1 \bar{L} P_R \phi L + Y_1^\dagger \bar{L} P_L \phi^\dagger L + Y_2 \bar{L} P_R \tilde{\phi} L + Y_2^\dagger \bar{L} P_L \tilde{\phi}^\dagger L) \int dy (Y_1 \bar{L} P_R \phi L + Y_1^\dagger \bar{L} P_L \phi^\dagger L + Y_2 \bar{L} P_R \tilde{\phi} L + Y_2^\dagger \bar{L} P_L \tilde{\phi}^\dagger L) a^\dagger(p_1) | 0 \rangle.$$

The amplitudes are acquired by evaluating all the contractions. Note, that since the mass eigenstates are mixings of the electroweak states, one gets effective couplings for the four neutral scalar states and the two Pseudoscalars in the form of:

$$\tilde{Y}_i = Y_1 O_{i1} + Y_2 O_{i2} + Y_L O_{i3} + Y_R O_{i4} \quad \text{with } i \in \{1, 2, 3, 4\} \quad (4.1)$$

and

$$\tilde{Y}'_i = Y_1 O'_{i1} + Y_2 O'_{i2} + Y_L O'_{i3} + Y_R O'_{i4} \quad \text{with } i \in \{3, 4\}, \quad (4.2)$$

with both  $O$  and  $O'$  being orthogonal matrices for scalars in eq. (4.1) and pseudoscalars in eq. (4.2). In eq. 4.2,  $i$  is only either 3 or 4, because the last two columns of  $O'$  are reserved for the pseudoscalar Higgs Bosons (see Appendix A.1). Keeping this in mind, the amplitudes for the scalar decay channel are as follows:

$$\begin{aligned} \mathcal{M}_S &= \sum_{i=1}^4 i \frac{\tilde{Y}_i^{e\mu} \tilde{Y}_i^{ee}}{-m_i^2} (\bar{u}_e(p_2)(P_L)u_\mu(p_1)) (\bar{u}_e(p_4)(P_L)v_e(p_3)) \\ &+ \sum_{i=1}^4 i \frac{\tilde{Y}_i^{e\mu} (\tilde{Y}_i^{ee})^*}{-m_i^2} (\bar{u}_e(p_2)(P_L)u_\mu(p_1)) (\bar{u}_e(p_4)(P_R)v_e(p_3)) \\ &+ \sum_{i=1}^4 i \frac{(\tilde{Y}_i^{\mu e})^* \tilde{Y}_i^{ee}}{-m_i^2} (\bar{u}_e(p_2)(P_R)u_\mu(p_1)) (\bar{u}_e(p_4)(P_L)v_e(p_3)) \\ &+ \sum_{i=1}^4 i \frac{(\tilde{Y}_i^{\mu e})^* (\tilde{Y}_i^{ee})^*}{-m_i^2} (\bar{u}_e(p_2)(P_R)u_\mu(p_1)) (\bar{u}_e(p_4)(P_R)v_e(p_3)) \end{aligned}$$

as well as for the pseudoscalar channel:

$$\begin{aligned}
 \mathcal{M}_P = & - \sum_{i=1}^2 i \frac{\widetilde{Y}'_i{}^{e\mu} \widetilde{Y}'_i{}^{ee}}{-m_{A_i}^2} (\bar{u}_e(p_2)(P_L)u_\mu(p_1)) (\bar{u}_e(p_4)(P_L)v_e(p_3)) \\
 & + \sum_{i=1}^2 i \frac{\widetilde{Y}'_i{}^{e\mu} (\widetilde{Y}'_i{}^{ee})^*}{-m_{A_i}^2} (\bar{u}_e(p_2)(P_L)u_\mu(p_1)) (\bar{u}_e(p_4)(P_R)v_e(p_3)) \\
 & + \sum_{i=1}^2 i \frac{(\widetilde{Y}'_i{}^{\mu e})^* \widetilde{Y}'_i{}^{ee}}{-m_{A_i}^2} (\bar{u}_e(p_2)(P_R)u_\mu(p_1)) (\bar{u}_e(p_4)(P_L)v_e(p_3)) \\
 & - \sum_{i=1}^2 i \frac{(\widetilde{Y}'_i{}^{\mu e})^* (\widetilde{Y}'_i{}^{ee})^*}{-m_{A_i}^2} (\bar{u}_e(p_2)(P_R)u_\mu(p_1)) (\bar{u}_e(p_4)(P_R)v_e(p_3))
 \end{aligned}$$

For the doubly charged decay channel, the following holds:

$$\begin{aligned}
 \mathcal{M}_2 = & \langle 0 | a(p_2)a^c(p_3)a(p_4) T \int dx \left( \frac{1}{2} Y_R L^T C P_R \Delta_R L + \frac{1}{2} Y_L^\dagger L^T C P_L \Delta_L^\dagger L \right) \\
 & \int dy \left( \frac{1}{2} Y_R L^T C P_R \Delta_R L + \frac{1}{2} Y_L^\dagger L^T C P_L \Delta_L^\dagger L \right) a^\dagger(p_1) | 0 \rangle \\
 = & i \frac{Y_L^{e\mu} Y_L^{ee}}{-m_L^{-2}} (v_e(p_3)^T (C P_L) u_\mu(p_1)) (\bar{u}_e(p_2) (C P_L) \bar{u}_e(p_4)^T) \\
 & + i \frac{(Y_R^{\mu e})^* (Y_R^{ee})^*}{-m_R^{-2}} (v_e(p_3)^T (C P_R) u_\mu(p_1)) (\bar{u}_e(p_2) (C P_R) \bar{u}_e(p_4)^T)
 \end{aligned}$$

Finally, there is another Feynman graph with switched out-states in the neutral decay channel:

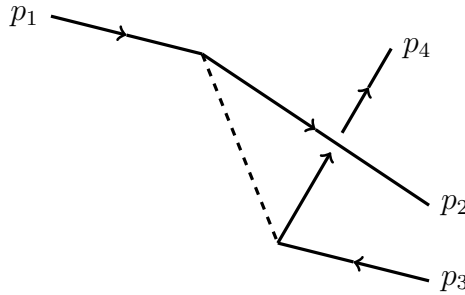


Figure 4.2.. neutral scalar decay channel with switched out-states  $\mathcal{M}_3$ .

For this part, it is important to note, that only  $p_2$  and  $p_4$  have to be switched. However, since switching two fermions, results in a change of sign, one ends up with the following

#### 4. Calculating The Decay

---

amplitude in the scalar case:

$$\begin{aligned}
\mathcal{M}_{\tilde{S}} = & - \sum_{i=1}^4 i \frac{\tilde{Y}_i^{e\mu} \tilde{Y}_i^{ee}}{-m_i^2} (\bar{u}_e(p_4)(P_L)u_\mu(p_1)) (\bar{u}_e(p_2)(P_L)v_e(p_3)) \\
& - \sum_{i=1}^4 i \frac{\tilde{Y}_i^{e\mu} (\tilde{Y}_i^{ee})^*}{-m_i^2} (\bar{u}_e(p_4)(P_L)u_\mu(p_1)) (\bar{u}_e(p_2)(P_R)v_e(p_3)) \\
& - \sum_{i=1}^4 i \frac{(\tilde{Y}_i^{\mu e})^* \tilde{Y}_i^{ee}}{-m_i^2} (\bar{u}_e(p_4)(P_R)u_\mu(p_1)) (\bar{u}_e(p_2)(P_L)v_e(p_3)) \\
& - \sum_{i=1}^4 i \frac{(\tilde{Y}_i^{\mu e})^* (\tilde{Y}_i^{ee})^*}{-m_i^2} (\bar{u}_e(p_4)(P_R)u_\mu(p_1)) (\bar{u}_e(p_2)(P_R)v_e(p_3)),
\end{aligned}$$

as well as for the Pseudoscalars:

$$\begin{aligned}
\mathcal{M}_{\tilde{P}} = & + \sum_{i=1}^2 i \frac{\tilde{Y}'_i{}^{e\mu} \tilde{Y}'_i{}^{ee}}{-m_{A_i}^2} (\bar{u}_e(p_4)(P_L)u_\mu(p_1)) (\bar{u}_e(p_2)(P_L)v_e(p_3)) \\
& - \sum_{i=1}^2 i \frac{\tilde{Y}'_i{}^{e\mu} (\tilde{Y}'_i{}^{ee})^*}{-m_{A_i}^2} (\bar{u}_e(p_4)(P_L)u_\mu(p_1)) (\bar{u}_e(p_2)(P_R)v_e(p_3)) \\
& - \sum_{i=1}^2 i \frac{(\tilde{Y}'_i{}^{\mu e})^* \tilde{Y}'_i{}^{ee}}{-m_{A_i}^2} (\bar{u}_e(p_4)(P_R)u_\mu(p_1)) (\bar{u}_e(p_2)(P_L)v_e(p_3)) \\
& + \sum_{i=1}^2 i \frac{(\tilde{Y}'_i{}^{\mu e})^* (\tilde{Y}'_i{}^{ee})^*}{-m_{A_i}^2} (\bar{u}_e(p_4)(P_R)u_\mu(p_1)) (\bar{u}_e(p_2)(P_R)v_e(p_3)).
\end{aligned}$$

Therefore, the full amplitude is as follows:

$$\begin{aligned}
\mathcal{M} = & \mathcal{M}_1 + \mathcal{M}_2 + \mathcal{M}_3 \\
= & \mathcal{M}_S + \mathcal{M}_P + \mathcal{M}_2 + \mathcal{M}_{\tilde{S}} + \mathcal{M}_{\tilde{P}}.
\end{aligned}$$

In order to obtain the decay width, the squared amplitudes have to be computed. Note, that after evaluating the traces, several terms proportional to  $m_e$  or higher orders of  $m_e$ , remain. Yet, these contributions are negligible, as  $m_e \ll m_\mu$ . Hence, the value of the squared amplitudes in the limit of  $m_e \rightarrow 0$  is

$$\begin{aligned}
|\overline{M}|^2 = & \left[ \sum_{i=1}^2 \left( \frac{(\tilde{Y}'_i{}^{e\mu})^* (\tilde{Y}'_i{}^{ee})^*}{m_{A_i}^2} \left( \frac{Y_R^{\mu e} Y_R^{ee}}{m_R^{-2}} + \frac{Y_L^{e\mu} Y_L^{ee}}{m_L^{-2}} \right) + \frac{\tilde{Y}'_i{}^{e\mu} \tilde{Y}'_i{}^{ee}}{m_{A_i}^2} \left( \frac{(Y_R^{\mu e})^* (Y_R^{ee})^*}{m_R^{-2}} + \frac{(Y_L^{e\mu})^* (Y_L^{ee})^*}{m_L^{-2}} \right) \right) \right. \\
& + \sum_{i=1}^4 \left( \frac{(\tilde{Y}_i{}^{e\mu})^* (\tilde{Y}_i{}^{ee})^*}{m_i^2} \left( \frac{Y_R^{\mu e} Y_R^{ee}}{m_R^{-2}} + \frac{Y_L^{e\mu} Y_L^{ee}}{m_L^{-2}} \right) + \frac{\tilde{Y}_i{}^{e\mu} \tilde{Y}_i{}^{ee}}{m_i^2} \left( \frac{(Y_R^{\mu e})^* (Y_R^{ee})^*}{m_R^{-2}} + \frac{(Y_L^{e\mu})^* (Y_L^{ee})^*}{m_L^{-2}} \right) \right) \\
& \cdot (2p_1 p_2 p_3 p_4 - 2p_1 p_4 p_2 p_3) \Big]
\end{aligned}$$

$$\begin{aligned}
 & + (2p_1 p_3 p_2 p_4) \left[ \left( \frac{(Y_L^{e\mu})^* (Y_L^{ee})^* Y_L^{e\mu} Y_L^{ee}}{m_L^{-2}} + \frac{Y_R^{\mu e} Y_R^{ee} (Y_R^{\mu e})^* (Y_R^{ee})^*}{m_R^{-2}} \right) \right. \\
 & + \sum_{i=1}^2 \sum_{j=1}^2 \left( \frac{\widetilde{Y}'_i{}^{\mu e} \widetilde{Y}'_i{}^{ee} (\widetilde{Y}'_j{}^{\mu e})^* (\widetilde{Y}'_j{}^{ee})^*}{m_{A_i}^2 m_{A_j}^2} + \frac{(\widetilde{Y}'_i{}^{e\mu})^* (\widetilde{Y}'_i{}^{ee})^* \widetilde{Y}'_j{}^{e\mu} \widetilde{Y}'_j{}^{ee}}{m_{A_i}^2 m_{A_j}^2} \right) \\
 & + \sum_{i=1}^4 \sum_{j=1}^2 \left( -\frac{(\widetilde{Y}_i{}^{e\mu})^* (\widetilde{Y}_i{}^{ee})^* \widetilde{Y}'_j{}^{e\mu} \widetilde{Y}'_j{}^{ee}}{m_i^2 m_{A_j}^2} - \frac{(\widetilde{Y}'_j{}^{e\mu})^* (\widetilde{Y}'_j{}^{ee})^* \widetilde{Y}_i{}^{e\mu} \widetilde{Y}_i{}^{ee}}{m_{A_j}^2 m_i^2} \right. \\
 & \left. - \frac{\widetilde{Y}'_j{}^{\mu e} \widetilde{Y}'_j{}^{ee} (\widetilde{Y}_i{}^{\mu e})^* (\widetilde{Y}_i{}^{ee})^*}{m_{A_j}^2 m_i^2} - \frac{\widetilde{Y}_i{}^{\mu e} \widetilde{Y}_i{}^{ee} (\widetilde{Y}'_j{}^{\mu e})^* (\widetilde{Y}'_j{}^{ee})^*}{m_{A_j}^2 m_i^2} \right) \\
 & \left. + \sum_{i=1}^4 \sum_{j=1}^4 \left( \frac{(\widetilde{Y}_i{}^{e\mu} \widetilde{Y}_i{}^{ee} (\widetilde{Y}'_j{}^{\mu e})^* (\widetilde{Y}'_j{}^{ee})^*}{m_i^2 m_j^2} + \frac{(\widetilde{Y}'_i{}^{e\mu})^* (\widetilde{Y}'_i{}^{ee})^* \widetilde{Y}_j{}^{e\mu} \widetilde{Y}_j{}^{ee}}{m_i^2 m_j^2} \right) \right] \\
 & + (2p_1 p_2 p_3 p_4 + 2p_1 p_4 p_3 p_2) \left[ \sum_{i=1}^4 \sum_{j=1}^4 \left( \frac{(\widetilde{Y}_i{}^{e\mu})^* \widetilde{Y}_i{}^{ee} \widetilde{Y}'_j{}^{e\mu} (\widetilde{Y}'_j{}^{ee})^*}{m_i^2 m_j^2} + \frac{\widetilde{Y}_i{}^{\mu e} (\widetilde{Y}'_i{}^{ee})^* (\widetilde{Y}'_j{}^{\mu e})^* \widetilde{Y}_j{}^{ee}}{m_i^2 m_j^2} \right) \right. \\
 & + \sum_{i=1}^2 \sum_{j=1}^4 \left( \frac{(\widetilde{Y}'_i{}^{e\mu})^* \widetilde{Y}'_i{}^{ee} \widetilde{Y}_j{}^{e\mu} (\widetilde{Y}'_j{}^{ee})^*}{m_{A_i}^2 m_j^2} + \frac{\widetilde{Y}'_i{}^{\mu e} (\widetilde{Y}'_i{}^{ee})^* (\widetilde{Y}'_j{}^{\mu e})^* \widetilde{Y}_j{}^{ee}}{m_{A_i}^2 m_j^2} \right. \\
 & \left. + \frac{(\widetilde{Y}_j{}^{e\mu})^* \widetilde{Y}_j{}^{ee} \widetilde{Y}'_i{}^{e\mu} (\widetilde{Y}'_i{}^{ee})^*}{m_j^2 m_{A_i}^2} + \frac{\widetilde{Y}_j{}^{\mu e} (\widetilde{Y}'_j{}^{ee})^* (\widetilde{Y}'_i{}^{\mu e})^* \widetilde{Y}_i{}^{ee}}{m_j^2 m_{A_i}^2} \right) \\
 & \left. + \sum_{i=1}^2 \sum_{j=1}^2 \left( \frac{(\widetilde{Y}'_i{}^{\mu e} (\widetilde{Y}'_i{}^{ee})^* (\widetilde{Y}'_j{}^{\mu e})^* \widetilde{Y}'_j{}^{ee}}{m_{A_i}^2 m_{A_j}^2} + \frac{(\widetilde{Y}'_i{}^{e\mu})^* \widetilde{Y}'_i{}^{ee} \widetilde{Y}'_j{}^{e\mu} (\widetilde{Y}'_j{}^{ee})^*}{m_{A_i}^2 m_{A_j}^2} \right) \right]
 \end{aligned} \tag{4.3}$$

Note, that this rather lengthy expression, only contains three different combinations of scalar products remain:

$$2p_1 p_2 p_3 p_4 + 2p_1 p_4 p_3 p_2 \tag{4.4}$$

$$2p_1 p_3 p_2 p_4 \tag{4.5}$$

$$2p_1 p_2 p_3 p_4 - 2p_1 p_4 p_3 p_2. \tag{4.6}$$

These can be expressed by Mandelstam variables, in order to perform phase space integration.

## 4.2. Rewriting The Traces

Consider a two-particle scattering process, the Mandelstam variables  $s, t$  and  $u$  are defined as follows [11]:

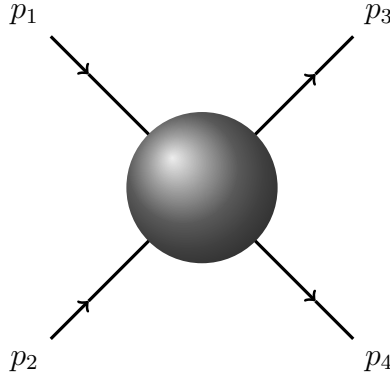


Figure 4.3.. two-particle scattering process where  $p_1$  and  $p_2$  are the in-states and  $p_3$  and  $p_4$  are out-states.

$$s = (p_1 + p_2)^2 = (p_3 + p_4)^2 \quad (4.7)$$

$$t = (p_1 - p_3)^2 = (p_2 - p_4)^2 \quad (4.8)$$

$$u = (p_1 - p_2)^2 = (p_2 - p_3)^2 \quad (4.9)$$

To obtain the Mandelstam variables  $\bar{s}, \bar{t}$  and  $\bar{u}$  in a three-particle scattering process, crossing symmetry can be used:

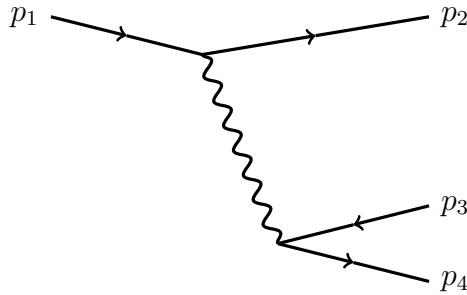


Figure 4.4.. Three-particle scattering process where  $p_1$  is the in-state and  $p_2, p_3$  and  $p_4$  are out-states.

$$\bar{s} := (p_2 + p_3)^2 = (p_1 - p_4)^2$$

$$\bar{t} := (p_3 + p_4)^2 = (p_1 - p_2)^2$$

$$\bar{u} := (p_2 + p_4)^2 = (p_1 - p_3)^2$$

These equations can be applied to eliminate the scalar products and express them as combinations of  $\bar{s}, \bar{t}$  and  $\bar{u}$ .

$$\begin{aligned}\bar{s} &= (p_1 - p_4)^2 = p_1^2 + p_4^2 - 2p_1p_4 = m_\mu^2 + m_e^2 - 2p_1p_4 = 2m_e^2 + 2p_2p_3 \\ \bar{t} &= (p_1 - p_2)^2 = p_1^2 + p_2^2 - 2p_1p_2 = m_\mu^2 + m_e^2 - 2p_1p_2 = 2m_e^2 + 2p_3p_4 \\ \bar{u} &= (p_1 - p_3)^2 = p_1^2 + p_3^2 - 2p_1p_3 = m_\mu^2 + m_e^2 - 2p_1p_3 = 2m_e^2 + 2p_2p_4,\end{aligned}$$

rearranging these expressions yields

$$\begin{aligned}p_1p_2 &= 1/2(m_\mu^2 + m_e^2 - \bar{t}) \\ p_1p_3 &= 1/2(m_\mu^2 + m_e^2 - \bar{u}) \\ p_1p_4 &= 1/2(m_\mu^2 + m_e^2 - \bar{s}) \\ p_2p_3 &= 1/2(\bar{s} - 2m_e^2) \\ p_3p_4 &= 1/2(\bar{t} - 2m_e^2) \\ p_2p_4 &= 1/2(\bar{u} - 2m_e^2)\end{aligned}$$

and also, the following equation holds. With this  $\bar{u}$  can be eliminated

$$\bar{u} = m_\mu^2 + 3m_e^2 - \bar{s} - \bar{t}.$$

Now, after letting  $m_e \rightarrow 0$

$$p_1p_2 = 1/2(m_\mu^2 - \bar{t}) \tag{4.10}$$

$$p_1p_3 = 1/2(m_\mu^2 - \bar{u}) \tag{4.11}$$

$$p_1p_4 = 1/2(m_\mu^2 - \bar{s}) \tag{4.12}$$

$$p_2p_3 = 1/2\bar{s} \tag{4.13}$$

$$p_3p_4 = 1/2\bar{t} \tag{4.14}$$

$$p_2p_4 = 1/2\bar{u} \tag{4.15}$$

$$\bar{u} = m_\mu^2 - \bar{s} - \bar{t} \tag{4.16}$$

remains. Inserting these expressions in eq. (4.5) to eliminate the scalar products yields

$$\begin{aligned}2p_1p_3p_2p_4 &= \frac{1}{2}((m_\mu^2 - \bar{u})\bar{u}) \\ &= \frac{1}{2}(-\bar{u}^2 + m_\mu^2\bar{u}) \\ &= \frac{1}{2}(-(m_\mu^2 - \bar{s} - \bar{t})^2 + m_\mu(m_\mu^2 - \bar{s} - \bar{t})) \\ &= \frac{1}{2}(-\bar{s}^2 - \bar{t}^2 + m_\mu^2(\bar{s} + \bar{t})).\end{aligned} \tag{4.17}$$

#### 4. Calculating The Decay

---

Furthermore, inserting these expressions in eq. (4.4) yields

$$\begin{aligned} 2p_1p_2p_3p_4 + 2p_1p_4p_3p_2 &= \frac{1}{2} \left( (m_\mu^2 - \bar{t})\bar{t} + (m_\mu^2 - \bar{s})\bar{s} \right) \\ &= \frac{1}{2} \left( -\bar{s}^2 - \bar{t}^2 + m_\mu^2(\bar{s} + \bar{t}) \right), \end{aligned} \quad (4.18)$$

and eq. (4.5)

$$\begin{aligned} 2p_1p_2p_3p_4 - 2p_1p_4p_3p_2 &= \frac{1}{2} \left( (m_\mu^2 - \bar{t})\bar{t} - (m_\mu^2 - \bar{s})\bar{s} \right) \\ &= \frac{1}{2} \left( \bar{t}^2 - \bar{s}^2 + m_\mu^2(\bar{t} - \bar{s}) \right) \end{aligned} \quad (4.19)$$

Conveniently, (4.17) has the same result as (4.18), so only two different integrals are left to compute. Now we need to perform the integration.

### 4.3. Phase Space Integration

In general, the differential decay width for a three particle decay process is given as (see Ref. [5])

$$\begin{aligned} d\Gamma &= \frac{|M|^2}{2m_\mu} \left( \frac{d^3p_2}{(2\pi)^3 2E_2} \right) \left( \frac{d^3p_3}{(2\pi)^3 2E_3} \right) \left( \frac{d^3p_4}{(2\pi)^3 E_4} \right) (2\pi)^4 \delta^4(p_1 - p_2 - p_3 - p_4) \\ &= \frac{1}{8(2\pi)^5 m_\mu} \frac{d^3p_2}{E_2} \frac{d^3p_3}{E_3} \frac{d^3p_4}{E_4} \delta^4(p_1 - p_2 - p_3 - p_4). \end{aligned}$$

The integrated decay width is thus:

$$\Rightarrow \Gamma = \frac{1}{8(2\pi)^5 m_\mu} \int_{-\infty}^{\infty} d^3p_2 d^3p_3 d^3p_4 \delta^4(p_1 - p_2 - p_3 - p_4) \frac{1}{E_2 E_3 E_4} |M|^2. \quad (4.20)$$

The following computation will be in large parts analogous to Ref. [13]. Note, that the following expressions are equal to 1:

$$\begin{aligned} 1 &= \int_{4m_e^2}^{(m_\mu - m_e)^2} d\bar{s} \delta(\bar{s} - (p_2 + p_3)^2) \\ 1 &= \int_{4m_e^2}^{(m_\mu - m_e)^2} d\bar{t} \delta(\bar{t} - (p_3 + p_4)^2). \end{aligned}$$

inserting these into the above equation, as well as using  $\delta(q^2 - m^2)\Theta(q_0)d^4q = \frac{d^3q}{(2\pi)^3 E(q)}$  yields

$$\begin{aligned}
 \Rightarrow \Gamma &= \frac{1}{8(2\pi)^5 m_\mu} \int_{-\infty}^{\infty} d^4p_2 d^4p_3 d^4p_4 \Theta(p_{20}) \Theta(p_{30}) \Theta(p_{40}) \delta^4(p_1 - p_2 - p_3 - p_4) \delta(p_2^2 - m_e^2) \\
 &\quad \delta(p_3^2 - m_e^2) \delta(p_4^2 - m_e^2) \int_{4m_e^2}^{(m_\mu - m_e)^2} d\bar{s} \int_{4m_e^2}^{(m_\mu - m_e)^2} d\bar{t} \delta(\bar{t} - (p_3 + p_4)^2) \delta(\bar{s} - (p_2 + p_3)^2) |\overline{M}|^2 \\
 &= \frac{1}{8(2\pi)^5 m_\mu} \int_{4m_e^2}^{(m_\mu - m_e)^2} d\bar{s} \int_{4m_e^2}^{(m_\mu - m_e)^2} d\bar{t} |\overline{M}|^2 I, \tag{4.21}
 \end{aligned}$$

where  $I$  is defined as:

$$\begin{aligned}
 I &= \int_{-\infty}^{\infty} d^4p_2 d^4p_3 d^4p_4 \Theta(p_{20}) \Theta(p_{30}) \Theta(p_{40}) \delta^4(p_1 - p_2 - p_3 - p_4) \delta(p_2^2 - m_e^2) \\
 &\quad \delta(p_3^2 - m_e^2) \delta(p_4^2 - m_e^2) \delta(\bar{t} - (p_3 + p_4)^2) \delta(\bar{s} - (p_2 + p_3)^2) \\
 &\quad \text{note that } d^4p_3 \text{ gets consumed by } \delta^4 \\
 \Rightarrow I &= \int_{-\infty}^{\infty} d^4p_2 d^4p_4 \Theta(p_{20}) \Theta(p_{10} - p_{20} - p_{40}) \Theta(p_{40}) \delta(p_2^2 - m_e^2) \\
 &\quad \delta((p_1 - p_2 - p_4)^2 - m_e^2) \delta(p_4^2 - m_e^2) \delta(\bar{t} - (p_3 + p_4)^2) \delta(\bar{s} - (p_2 + p_3)^2). \tag{4.22}
 \end{aligned}$$

When computing  $I$ , consider the  $\mu$  resting frame

$$p_1 = \begin{pmatrix} m_\mu \\ \vec{0} \end{pmatrix}.$$

Switching to the following frame facilitates these expressions:

$$\begin{aligned}
 (p_2 + p_3)^2 &= (p_1 - p_4)^2 = m_\mu^2 + m_e^2 - 2p_{10}p_{40} \\
 p_3^2 &= (p_1 - p_2 - p_4)^2 = m_\mu^2 + (p_2 + p_4)^2 - 2p_{10}(p_{20} + p_{40}) \\
 &= m_\mu^2 + 2m_e^2 - 2(\vec{p}_2 \cdot \vec{p}_4) - 2p_{10}(p_{20} + p_{40}) \\
 (p_3 - p_4)^2 &= (p_1 - p_2)^2 = m_\mu^2 + m_e^2 - 2p_{10}p_{20},
 \end{aligned}$$

#### 4. Calculating The Decay

---

with the new definitions:

$$\begin{aligned}
|\vec{p}_2| &:= p \\
|\vec{p}_4| &:= q \\
(\vec{p}_2\vec{p}_4) &:= pq \cos \alpha \\
\Rightarrow I &= \int_{-\infty}^{\infty} d^4 p_2 \Theta(p_{20}) \delta(p_2^2 - m_e^2) \delta(\bar{t} - m_\mu^2 - m_e^2 + 2p_{10}p_{40}) \\
&\stackrel{\Theta(p_{10}-p_{20}-p_{40})}{\rightarrow} \int_0^{p_{10}-p_{20}} dp_{40} \delta(\bar{s} - m_\mu^2 - m_e^2 + 2p_{10}p_{40}) \int_0^{\Theta(p_{40})} dq q^2 \delta(\underbrace{p_{40}^2 - q^2}_{p_4^2} - m_e^2) \cdot 2\pi \\
&\int_1^{-1} d(\cos \alpha) \delta(m_\mu^2 + m_e^2 - 2p_{10}(p_{20} + p_{40}) - 2pq \cos \alpha). \tag{4.23}
\end{aligned}$$

The  $2\pi$  stems from integrating over the azimuth angle. Evaluating these Integrals is can be achieved by applying this expression:

$$\delta(g(x)) = \sum_i \frac{\delta(x - x_i)}{|g'(x_i)|}. \tag{4.24}$$

In the case of the distributions in eq. (4.23), this results in the following form

$$\begin{aligned}
\delta(-q^2 - (p_{40}^2 - m_e^2)) &\Rightarrow g(q) = -(-q^2 - (p_{40}^2 - m_e^2)) = \left[ (q - \sqrt{p_{40}^2 - m_e^2})(q + \sqrt{p_{40}^2 - m_e^2}) \right] \\
g'(q) &= -2q \\
\Rightarrow \delta(p_{40}^2 - q^2 - m_e^2) &= \frac{\left[ \delta(q - \sqrt{p_{40}^2 - m_e^2}) + \delta(q + \sqrt{p_{40}^2 - m_e^2}) \right]}{2\sqrt{p_{40}^2 - m_e^2}}. \tag{4.25}
\end{aligned}$$

Since the lower limit of the integral along  $dq$  is 0,  $\int_0^\infty dq \delta(q - \sqrt{p_{40}^2 - m_e^2})$  will vanish. Now, what remains is this:

$$\begin{aligned}
\Rightarrow I &= \pi \int_{-\infty}^{\infty} d^4 p_2 \Theta(p_{20}) \delta(p_2^2 - m_e^2) \delta(\bar{t} - m_\mu^2 - m_e^2 + 2p_{10}p_{40}) \\
&\int_0^{p_{10}-p_{20}} dp_{40} \delta(\bar{s} - m_\mu^2 - m_e^2 + 2p_{10}p_{40}) \int_0^\infty dq \frac{q}{p} \frac{1}{2\sqrt{p_{40}^2 - m_e^2}} \delta\left(q - \sqrt{p_{40}^2 - m_e^2}\right).
\end{aligned}$$

Likewise with eq. (4.24), the following holds:

$$\delta(m_\mu^2 + m_e^2 - 2p_{10}(p_{20} + p_{40}) - 2pq \cos \alpha) = \delta(g(\cos \alpha)) = \frac{\delta(\cos \alpha - 0)}{2pq} = \frac{\delta(\cos \alpha)}{2pq}.$$

This consumes the  $d \cos \alpha$  Integral and renders  $q^2 \Rightarrow \frac{q}{p}$ . Also,

$$\Rightarrow \delta(\bar{s} - m_\mu^2 - m_e^2 + 2p_{10}p_{40}) = \delta(g(p_{40})) = \frac{\delta(p_{40})}{2p_{10}}. \quad (4.26)$$

$\Rightarrow$  consumes the  $p_{40}$  integration and gives  $\frac{1}{2p_{10}}$  as

$$\int_0^\infty dq \frac{q}{p} \frac{1}{2\sqrt{p_{40}^2 - m_e^2}} \delta\left(q - \sqrt{p_{40}^2 - m_e^2}\right) = \frac{\sqrt{p_{40}^2 - m_e^2}}{2p\sqrt{p_{40}^2 - m_e^2}} = \frac{1}{2p}.$$

$$\begin{aligned} \Rightarrow I &= \pi \int_{-\infty}^\infty d^4 p_2 \Theta(p_{20}) \delta(p_2^2 - m_e^2) \delta(\bar{t} - m_\mu^2 - m_e^2 + 2p_{10}p_{40}) \frac{1}{2p_{10}} \frac{1}{2p} \\ &= \frac{\pi}{4p_{10}} \underbrace{\int_{-\infty}^\infty dp_{20} \delta(\bar{t} - m_\mu^2 - m_e^2 + 2p_{10}p_{40})}_{\substack{\text{analogus to (4.26)} \\ \Rightarrow \frac{1}{2p_{10}}}} \cdot \underbrace{4\pi}_{\text{solid angle}} \cdot \underbrace{\int_0^\infty dp \frac{p^2}{p} \delta(p_2^2 - p^2 - m_e^2)}_{\text{analogus to (4.25)}} \end{aligned}$$

Inserting this into the above eq. (4.21) yields

$$\begin{aligned} \Rightarrow I &= \frac{\pi^2}{2p_{10}^2} \int_0^\infty dp \frac{p}{2\sqrt{p_{20}^2 - m_e^2}} \delta\left(p - \sqrt{p_{20}^2 - m_e^2}\right) \\ &= \frac{\pi^2}{4p_{10}^2} \frac{\sqrt{p_{20}^2 - m_e^2}}{\sqrt{p_{20}^2 - m_e^2}} \\ &= \frac{\pi^2}{4p_{10}^2} \\ \Rightarrow \Gamma &= \frac{1}{8(2\pi)^5 m_\mu} \frac{\pi^2}{4p_{10}^2} \int d\bar{s} d\bar{t} |\overline{M}|^2. \quad (4.27) \end{aligned}$$

Note, that in the muon resting frame  $p_{10}^2 = m_\mu^2$ , which leaves us with the expression for the decay width only dependent on an integration along two Mandelstam variables.

$$\Rightarrow \Gamma = \frac{1}{8(2\pi)^5} \frac{\pi^2}{4m_\mu^3} \int d\bar{s} d\bar{t} |\overline{M}|^2. \quad (4.28)$$

So far, the limits are not identified.

### Evaluating Integration Limits

In order to find the limits of the  $\bar{t}$  and the  $\bar{s}$  integral, consider the system where  $\vec{p}_1 = \vec{p}_4$  holds. Here, we introduce the following redefinitions

$$\begin{aligned} |\vec{p}_2| &:= p \\ |\vec{p}_4| &:= q \\ \vec{p}_2 \vec{p}_4 &= pq \cos \alpha, \end{aligned}$$

which enables us to return to eq. (4.22) and rewrite it as follows:

$$\begin{aligned} \Rightarrow I &= \int_{-\infty}^{\infty} d^4 p_2 d^4 p_4 \Theta(p_{10} - p_{20} - p_{40}) \Theta(p_{40}) \delta(p_2^2 - m_e^2) \delta((p_1 - p_2 - p_4)^2 - m_e^2) \delta(p_4^2 - m_e^2) \\ &\quad \cdot \delta(\bar{s} - (p_1 - p_4)^2) \delta(\bar{t} - (p_1 - p_4)^2) \\ &= \int_{-\infty}^{\infty} d^4 p_4 \Theta(p_{40}) \delta(p_4^2 - m_e^2) \delta(\bar{s} - (p_1 - p_4)^2) I'. \end{aligned}$$

By way of the above definitions, one can obtain the following expression:

$$\begin{aligned} I' &= \int_{-\infty}^{\infty} dp_{20} \delta(m_\mu^2 + m_e^2 - 2p_{10}p_{20} - 2p_{10}p_{40} + 2p_{20}p_{40} + 2q^2) \Theta(p_{20}) \Theta(p_{10} - p_{20} - p_{40}) \\ &\quad \int_0^{\infty} dp p^2 \delta(p_{20}^2 - p^2 - m_e^2) \cdot 2\pi \int_{-1}^1 d(\cos \alpha) \delta(\bar{t} - m_\mu^2 - m_e^2 + 2p_{10}p_{20} - 2pq \cos \alpha). \end{aligned}$$

In case  $|\bar{t} - m_\mu^2 - m_e^2 + 2p_{10}p_{20}| \leq 2pq$ , with eq. (4.24), one can obtain

$$\begin{aligned} \delta(\bar{t} - m_\mu^2 - m_e^2 - 2p_{10}p_{40} - 2pq \cos \alpha) &= \frac{\delta(\cos \alpha)}{2pq} \\ \Rightarrow I' &= \int_{-\infty}^{\infty} \delta(m_\mu^2 + m_e^2 - 2p_{10}p_{20} - 2p_{10}p_{40} + 2p_{20}p_{40} - 2q^2) \\ &\quad \int_0^{\infty} dp p^2 \frac{\pi}{pq} \delta(p_{20}^2 - p^2 - m_e^2) \Theta(p_{20}) \Theta(p_{10} - p_{20} - p_{40}). \end{aligned}$$

With another application of eq. (4.24) one can also obtain:

$$\delta(m_\mu^2 + m_e^2 - 2p_{10}p_{40} + 2q^2 - 2p_{20}(p_{10} - p_{40})) = \frac{\delta(p_{20})}{2(p_{10} - p_{40})}.$$

The integral along  $dp_{20}$  can now be consumed by above  $\delta$ , as well as the integration along  $dp$  can be performed analogous to (4.25):

$$\begin{aligned} I' &= \int_{-\infty}^{\infty} dp_{20} \delta(m_\mu^2 + m_e^2 - 2p_{10}p_{20} + 2p_{20}p_{40} - 2p_{10}p_{40} + 2q^2) \\ &\quad \cdot \int_0^{\infty} dp \frac{p}{q} \pi \delta(p_{20}^2 - p^2 - m_e^2) \Theta(p_{20}) \Theta(p_{10} - p_{20} - p_{40}) \\ &= \frac{\pi}{2q(p_{10} - p_{40})} \int_0^{\infty} dp \frac{p}{2\sqrt{p_{20} - m_e^2}} \delta\left(p - \sqrt{p_{20} - m_e^2}\right) \Theta(p_{20}) \Theta(p_{10} - p_{20} - p_{40}) \\ &= \frac{\pi}{4q(p_{10} - p_{40})} \Theta(p_{20}) \Theta(p_{10} - p_{20} - p_{40}). \end{aligned} \tag{4.29}$$

This only holds if

$$p^2 = p_{20}^2 - m_e^2 \tag{4.30}$$

$$p_{20} = \frac{1}{2(p_{10} - p_{40})} (m_\mu^2 + m_e^2 - 2p_{10}p_{40} + 2q^2). \tag{4.31}$$

Thus  $I' = 0$ , and also if

$$\begin{aligned} p_{40} &= \frac{-1}{2p_{10}} (\bar{s} - m_\mu^2 - m_e^2 - 2q^2) \\ \Rightarrow I &= \int_{-\infty}^{\infty} d^4 p_4 \Theta(p_{40}) \delta(p_4^2 - m_e^2) \delta(\bar{s} - m_\mu^2 - m_e^2 + 2p_{10}p_{40}) I'. \end{aligned} \tag{4.32}$$

#### 4. Calculating The Decay

---

Inserting eq. (4.29) into above equation yields:

$$\begin{aligned} \Rightarrow I &= \frac{\pi}{2(p_{10} - p_{40})} \cdot 4\pi \int_0^\infty dp_{40} \int_0^\infty dq q^2 \delta(p_{40}^2 - q^2 - m_e^2) \Theta(p_{20}) \Theta(p_{40}) \\ &\quad \Theta(p_{10} - p_{20} - p_{40}) \underbrace{\delta(\bar{s} - m_\mu^2 - m_e^2 + 2p_{20}p_{40})}_{\text{consumes } p_{20} \text{ integral, yields } \frac{1}{2p_{20}}} \\ \Rightarrow I &= \frac{\pi^2}{2p_{10}} \int_0^\infty dq^2 \underbrace{\delta(p_{40}^2 - q^2 - m_e^2)}_{\delta(-(q^2 + m_e^2 - p_{40}^2))} \Theta(p_{20}) \Theta(p_{40}) \Theta(p_{10} - p_{20} - p_{40}) \frac{1}{p_{10} - p_{40}}. \end{aligned}$$

Thus, the  $\delta$  is giving this constraint:

$$p_{40}^2 - q^2 - m_e^2 = 0. \quad (4.33)$$

Additionally, with the definition of  $p_1$  according to the chosen frame:

$$\begin{aligned} p_1 &= \begin{pmatrix} p_{10} \\ \vec{q} \end{pmatrix} \\ \Rightarrow p_1^2 &= m_\mu^2 = p_{10}^2 - q^2 \\ \Rightarrow p_{10}^2 &= q^2 + m_\mu^2, \end{aligned} \quad (4.34)$$

and with eq. (4.32), (4.33) and (4.34) the following can be computed as

$$\begin{aligned} p_{40}^2 - q^2 - m_e^2 &= 0 \\ \Leftrightarrow p_{40}^2 &= \frac{1}{4(q^2 + m_\mu^2)} (\bar{s} - m_\mu^2 - m_e^2 - 2q^2) \\ \Leftrightarrow q^2 &= \frac{1}{4\bar{s}} [\bar{s}^2 - 2\bar{s}(m_\mu^2 + m_e^2) + (m_\mu^4 + m_e^4 - 2m_e^2 m_\mu^2)] \\ \Leftrightarrow q^2 &= \frac{1}{4\bar{s}} [\bar{s}^2 - 2\bar{s}(m_\mu^2 + m_e^2) + (m_\mu^2 - m_e^2)^2]. \end{aligned} \quad (4.35)$$

Including the definitions from before, one can simplify:

$$\begin{aligned} p_{10}^2 &= q^2 + m_\mu^2 \\ &= \frac{1}{4\bar{s}} [\bar{s}^2 - 2\bar{s}(m_\mu^2 + m_e^2) + (m_\mu^2 - m_e^2)^2] + m_\mu^2 \\ &= \frac{1}{4\bar{s}} [\bar{s}^2 + 2\bar{s}^2 m_\mu^2 - 2\bar{s} m_e^2 + m_\mu^4 + m_e^4 - 2m_e^2 m_\mu^2] \\ &= \frac{1}{4\bar{s}} [(\bar{s} + m_\mu^2 - m_e^2)^2] \\ \Rightarrow p_{10} &= \frac{1}{2\sqrt{\bar{s}}} (\bar{s} + m_\mu^2 - m_e^2). \end{aligned} \quad (4.36)$$

Inserting this result for  $p_{10}$  into eq. (4.32) yields

$$\begin{aligned} \Rightarrow p_{40} &= \frac{-1}{2\frac{1}{2\sqrt{s}}(\bar{s} + m_\mu^2 - m_e^2)} (\bar{s} - m_\mu^2 - m_e^2 - sq^2) \\ &= \frac{-\sqrt{s}(\bar{s} - m_\mu^2 - m_e^2 - 2q^2)}{(\bar{s} + m_\mu^2 - m_e^2)}. \end{aligned}$$

Applying eq. (4.35) into the above equation gives the following result for  $p_{40}$ :

$$\Rightarrow p_{40} = \frac{-1}{2\sqrt{s}} (\bar{s} - m_\mu^2 + m_e^2). \quad (4.37)$$

Upon inserting this into eq. (4.31), one finds

$$p_{20} = \frac{1}{2(p_{10} - p_{40})} (m_\mu^2 + m_e^2 - 2p_{10}p_{40} + 2q^2) \quad (4.38)$$

$$\begin{aligned} p_{20} &= \frac{\left( m_\mu^2 + m_e^2 - \frac{-2(\bar{s} + m_\mu^2 - m_e^2)(\bar{s} + m_e^2 - m_\mu^2)}{4\bar{s}} \right) + 2q^2}{2\frac{1}{2\sqrt{s}}(\bar{s} + m_\mu^2 - m_e^2 + \bar{s} + m_e^2 - m_\mu^2)} \\ \Rightarrow p_{20} &= \frac{\sqrt{\bar{s}}}{2}. \end{aligned} \quad (4.39)$$

Inserting eq. (4.30) again into eq. (4.39) gives the following result

$$p^2 = \frac{\bar{s}}{4} + m_e^2, \quad (4.40)$$

which in combination with eq. (4.35) yields,

$$\Rightarrow 2pq = 2\sqrt{\frac{\bar{s}}{4} + m_e^2} \sqrt{\frac{1}{4\bar{s}} \left[ \bar{s}^2 - 2\bar{s}(m_\mu^2 + m_e^2) + (m_\mu^2 - m_e^2)^2 \right]}.$$

We define  $\lambda$  as

$$\lambda[x, y, z] := x^2 + y^2 + z^2 - 2(xy + xz + yz),$$

in order to rewrite the expression from above in the following form:

$$\Rightarrow 2qp = \sqrt{\frac{\lambda[\bar{s}, m_e^2, m_\mu^2]}{\bar{s}}} \left( \frac{\bar{s}}{4} - m_e^2 \right). \quad (4.41)$$

#### 4. Calculating The Decay

This can be used to end this rather lengthy computation and find the integration limits using the inequality.

$$\begin{aligned} |\bar{t} - m_\mu^2 - m_e^2 + 2p_{10}p_{20}| &\leq 2pq \\ \Rightarrow |\bar{t} - \frac{1}{2}m_\mu^2 - \frac{3}{2}m_e^2 + \frac{1}{2}| &\leq \sqrt{\frac{\lambda[\bar{s}, m_e^2, m_\mu^2]}{\bar{s}} \left(\frac{\bar{s}}{4} - m_e^2\right)}. \end{aligned}$$

Finally, with the different cases of the inequality, we end up with:

$$\begin{aligned} \bar{s}_{\min} &= 4m_e \\ \bar{s}_{\max} &= (m_\mu^2 - m_e^2) \\ \bar{t}_{\min} &= m_\mu^2 + m_e^2 - \frac{1}{2}(\bar{s} + m_\mu^2 - m_e^2) - \sqrt{\frac{\lambda[\bar{s}, m_\mu^2, m_e^2]}{\bar{s}} \left(\frac{\bar{s}}{4} - m_e^2\right)} \\ \bar{t}_{\max} &= m_\mu^2 + m_e^2 - \frac{1}{2}(\bar{s} + m_\mu^2 - m_e^2) + \sqrt{\frac{\lambda[\bar{s}, m_\mu^2, m_e^2]}{\bar{s}} \left(\frac{\bar{s}}{4} - m_e^2\right)}. \end{aligned}$$

Note, that  $m_e \rightarrow 0$  has yet to be applied. Otherwise, the  $\bar{s}$  integration leads to elliptic integrals whose evaluation turns out to be rather non-trivial. Fortunately, this is not the case here. After letting  $m_e \rightarrow 0$  yields:

$$\bar{t}_{\min} = -\sqrt{\frac{(m_\mu^2 - \bar{s})^2}{4}} + \frac{1}{2}(m_\mu^2 - \bar{s}) = 0 \quad (4.42)$$

$$\bar{t}_{\max} = +\sqrt{\frac{(m_\mu^2 - \bar{s})^2}{4}} + \frac{1}{2}(m_\mu^2 - \bar{s}) = (m_\mu^2 - \bar{s}) \quad (4.43)$$

$$\bar{s}_{\min} = 0 \quad (4.44)$$

$$\bar{s}_{\max} = m_\mu^2. \quad (4.45)$$

Eventually we have all the tools to integrate the decay width

$$\Gamma = \frac{1}{32(2\pi)^5} \frac{\pi^2}{m_\mu^3} \int_{\bar{s}_{\min}}^{\bar{s}_{\max}} d\bar{s} \int_{\bar{t}_{\min}}^{\bar{t}_{\max}} dt |\overline{M}|^2. \quad (4.46)$$

## 4.4. Evaluating Integrals

With these limits, both integrals that need to be evaluated are:

$$\begin{aligned}
I_{(1)} &= \int_{\bar{s}_{min}}^{\bar{s}_{max}} d\bar{s} \int_{\bar{t}_{min}}^{\bar{t}_{max}} d\bar{t} \frac{1}{2} (-\bar{s}^2 - \bar{t}^2 + m_\mu^2(\bar{s} + \bar{t})) \\
&= \frac{m_\mu^8}{12} \\
I_{(3)} &= \int_{\bar{s}_{min}}^{\bar{s}_{max}} d\bar{s} \int_{\bar{t}_{min}}^{\bar{t}_{max}} d\bar{t} \frac{1}{2} (\bar{t}^2 - \bar{s}^2 + m_\mu^2(\bar{t} - \bar{s})) \\
&= \int_{\bar{s}_{min}}^{\bar{s}_{max}} d\bar{s} \frac{1}{6} (m_\mu^2 - \bar{s})(5m_\mu^4 - 13m_\mu^2\bar{s} - 4\bar{s}^2) \\
&= \frac{1}{6} (5m_\mu^8 - 9m_\mu^8 + 3m_\mu^8 + m_\mu^8) \\
&= 0.
\end{aligned}$$

This implies that, in the limit of  $m_e \rightarrow 0$ , the contribution from interference with doubly charged and neutral scalars vanishes. Inserting these results into eq. (4.3) yields the following:

$$\begin{aligned}
\int |\overline{M}|^2 &= \frac{m_\mu^8}{12} \left[ \frac{(Y_L^{e\mu})^* (Y_L^{ee})^* Y_L^{e\mu} Y_L^{ee}}{m_L^{-2} m_L^{-2}} + \frac{Y_R^{\mu e} Y_R^{ee} (Y_R^{\mu e})^* (Y_R^{ee})^*}{m_R^{-2} m_R^{-2}} \right. \\
&+ \sum_{i=1}^2 \sum_{j=1}^2 \left( \frac{(\widetilde{Y}'_i{}^{\mu e} \widetilde{Y}'_i{}^{ee} (\widetilde{Y}'_j{}^{\mu e})^* (\widetilde{Y}'_j{}^{ee})^*)}{m_{A_i}^2 m_{A_j}^2} + \frac{(\widetilde{Y}'_i{}^{e\mu})^* (\widetilde{Y}'_i{}^{ee})^* \widetilde{Y}'_j{}^{e\mu} \widetilde{Y}'_j{}^{ee}}{m_{A_i}^2 m_{A_j}^2} \right) \\
&+ \sum_{i=1}^4 \sum_{j=1}^4 \left( \frac{(\widetilde{Y}_i{}^{e\mu} \widetilde{Y}_i{}^{ee} (\widetilde{Y}_j{}^{\mu e})^* (\widetilde{Y}_j{}^{ee})^*)}{m_i^2 m_j^2} + \frac{(\widetilde{Y}_i{}^{e\mu})^* (\widetilde{Y}_i{}^{ee})^* \widetilde{Y}_j{}^{e\mu} \widetilde{Y}_j{}^{ee}}{m_i^2 m_j^2} \right) \\
&+ \sum_{i=1}^4 \sum_{j=1}^4 \left( \frac{(\widetilde{Y}_i{}^{e\mu})^* \widetilde{Y}_i{}^{ee} \widetilde{Y}_j{}^{e\mu} (\widetilde{Y}_j{}^{ee})^*}{m_i^2 m_j^2} + \frac{\widetilde{Y}_i{}^{\mu e} (\widetilde{Y}_i{}^{ee})^* (\widetilde{Y}_j{}^{\mu e})^* \widetilde{Y}_j{}^{ee}}{m_i^2 m_j^2} \right) \\
&+ \sum_{i=1}^2 \sum_{j=1}^2 \left( \frac{(\widetilde{Y}'_i{}^{\mu e} (\widetilde{Y}'_i{}^{ee})^* (\widetilde{Y}'_j{}^{\mu e})^* \widetilde{Y}'_j{}^{ee}}{m_{A_i}^2 m_{A_j}^2} + \frac{(\widetilde{Y}'_i{}^{e\mu})^* \widetilde{Y}'_i{}^{ee} \widetilde{Y}'_j{}^{e\mu} (\widetilde{Y}'_j{}^{ee})^*}{m_{A_i}^2 m_{A_j}^2} \right) \\
&+ \frac{m_\mu^8}{12} \left[ \sum_{i=1}^2 \sum_{j=1}^4 \left( \frac{(\widetilde{Y}'_i{}^{e\mu})^* \widetilde{Y}'_i{}^{ee} \widetilde{Y}_j{}^{e\mu} (\widetilde{Y}_j{}^{ee})^*}{m_{A_i}^2 m_j^2} + \frac{\widetilde{Y}'_i{}^{\mu e} (\widetilde{Y}'_i{}^{ee})^* (\widetilde{Y}_j{}^{\mu e})^* \widetilde{Y}_j{}^{ee}}{m_{A_i}^2 m_j^2} \right) \right. \\
&+ \left. \frac{(\widetilde{Y}_j{}^{e\mu})^* \widetilde{Y}_j{}^{ee} \widetilde{Y}'_i{}^{e\mu} (\widetilde{Y}'_i{}^{ee})^*}{m_j^2 m_{A_i}^2} + \frac{\widetilde{Y}_j{}^{\mu e} (\widetilde{Y}_j{}^{ee})^* (\widetilde{Y}'_i{}^{\mu e})^* \widetilde{Y}'_i{}^{ee}}{m_j^2 m_{A_i}^2} \right)
\end{aligned}$$

#### 4. Calculating The Decay

$$+ \sum_{i=1}^4 \sum_{j=1}^2 \left( -\frac{(\widetilde{Y}_i^{e\mu})^* (\widetilde{Y}_i^{ee})^* \widetilde{Y}'_j{}^{e\mu} \widetilde{Y}'_j{}^{ee}}{m_i^2 m_{A_j}^2} - \frac{(\widetilde{Y}'_j{}^{e\mu})^* (\widetilde{Y}'_j{}^{ee})^* \widetilde{Y}_i{}^{e\mu} \widetilde{Y}_i{}^{ee}}{m_{A_j}^2 m_i^2} - \frac{\widetilde{Y}'_j{}^{\mu e} \widetilde{Y}'_j{}^{ee} (\widetilde{Y}_i{}^{\mu e})^* (\widetilde{Y}_i{}^{ee})^*}{m_i^2 m_{A_j}^2} - \frac{\widetilde{Y}_i{}^{\mu e} \widetilde{Y}_i{}^{ee} (\widetilde{Y}'_j{}^{\mu e})^* (\widetilde{Y}'_j{}^{ee})^*}{m_i^2 m_{A_j}^2} \right).$$

The last bracket is still worrisome, as it describes non-vanishing interaction between scalar and pseudoscalar particles. However, in the limit of real Yukawa couplings and additionally renaming summation indices, these parts cancel each other out.

$$\begin{aligned} \int |\overline{M}|^2 &= \frac{m_\mu^8}{12} \left[ \frac{Y_L^{e\mu} Y_L^{ee}}{m_L^{-2}} \frac{Y_L^{e\mu} Y_L^{ee}}{m_L^{-2}} + \frac{Y_R^{\mu e} Y_R^{ee}}{m_R^{-2}} \frac{Y_R^{\mu e} Y_R^{ee}}{m_R^{-2}} \right. \\ &+ 2 \sum_{i=1}^4 \sum_{j=1}^4 \left( \frac{\widetilde{Y}_i{}^{e\mu} \widetilde{Y}_i{}^{ee} \widetilde{Y}_j{}^{e\mu} \widetilde{Y}_j{}^{ee}}{m_i^2 m_j^2} + \frac{\widetilde{Y}_i{}^{\mu e} \widetilde{Y}_i{}^{ee} \widetilde{Y}_j{}^{\mu e} \widetilde{Y}_j{}^{ee}}{m_i^2 m_j^2} \right) \\ &+ 2 \sum_{i=1}^2 \sum_{j=1}^2 \left( \frac{\widetilde{Y}'_i{}^{\mu e} \widetilde{Y}'_i{}^{ee} \widetilde{Y}'_j{}^{\mu e} \widetilde{Y}'_j{}^{ee}}{m_{A_i}^2 m_{A_j}^2} + \frac{\widetilde{Y}'_i{}^{e\mu} \widetilde{Y}'_i{}^{ee} \widetilde{Y}'_j{}^{e\mu} \widetilde{Y}'_j{}^{ee}}{m_{A_i}^2 m_{A_j}^2} \right) \left. \right] \\ &+ \frac{m_\mu^8}{12} \left[ \sum_{i=1}^2 \sum_{j=1}^4 \left( \underbrace{\frac{\widetilde{Y}'_i{}^{e\mu} \widetilde{Y}'_i{}^{ee} \widetilde{Y}_j{}^{e\mu} \widetilde{Y}_j{}^{ee}}{m_{A_i}^2 m_j^2} - \frac{\widetilde{Y}'_i{}^{e\mu} \widetilde{Y}'_i{}^{ee} \widetilde{Y}_j{}^{e\mu} \widetilde{Y}_j{}^{ee}}{m_{A_i}^2 m_j^2}}_{=0} \right. \right. \\ &+ \underbrace{\frac{\widetilde{Y}'_i{}^{\mu e} \widetilde{Y}'_i{}^{ee} \widetilde{Y}_j{}^{\mu e} \widetilde{Y}_j{}^{ee}}{m_{A_i}^2 m_j^2} - \frac{\widetilde{Y}'_i{}^{\mu e} \widetilde{Y}'_i{}^{ee} \widetilde{Y}_j{}^{\mu e} \widetilde{Y}_j{}^{ee}}{m_{A_i}^2 m_j^2}}_{=0} \\ &+ \left. \left. \underbrace{\frac{\widetilde{Y}_j{}^{e\mu} \widetilde{Y}_j{}^{ee} \widetilde{Y}'_i{}^{e\mu} \widetilde{Y}'_i{}^{ee}}{m_j^2 m_{A_i}^2} - \frac{\widetilde{Y}_j{}^{e\mu} \widetilde{Y}_j{}^{ee} \widetilde{Y}'_i{}^{e\mu} \widetilde{Y}'_i{}^{ee}}{m_j^2 m_{A_i}^2}}_{=0} + \underbrace{\frac{\widetilde{Y}_j{}^{\mu e} \widetilde{Y}_j{}^{ee} \widetilde{Y}'_i{}^{\mu e} \widetilde{Y}'_i{}^{ee}}{m_j^2 m_{A_i}^2} - \frac{\widetilde{Y}_j{}^{\mu e} \widetilde{Y}_j{}^{ee} \widetilde{Y}'_i{}^{\mu e} \widetilde{Y}'_i{}^{ee}}{m_j^2 m_{A_i}^2}}_{=0} \right) \right]. \end{aligned}$$

Thus, the total decay-width in the limit of real Yukawa couplings as well as  $m_e \rightarrow 0$ , takes this rather concise form:

$$\begin{aligned} \Gamma &= \frac{m_\mu^5}{3 \cdot 2^{12} \pi^2} \left[ \left( \frac{Y_L^{e\mu} Y_L^{ee}}{m_L^{-2}} \right)^2 + \left( \frac{Y_R^{\mu e} Y_R^{ee}}{m_R^{-2}} \right)^2 \right. \\ &+ 2 \sum_{i=1}^4 \sum_{j=1}^4 \left( \frac{\widetilde{Y}_i{}^{e\mu} \widetilde{Y}_i{}^{ee} \widetilde{Y}_j{}^{e\mu} \widetilde{Y}_j{}^{ee}}{m_i^2 m_j^2} + \frac{\widetilde{Y}_i{}^{\mu e} \widetilde{Y}_i{}^{ee} \widetilde{Y}_j{}^{\mu e} \widetilde{Y}_j{}^{ee}}{m_i^2 m_j^2} \right) \\ &+ 2 \sum_{i=1}^2 \sum_{j=1}^2 \left( \frac{\widetilde{Y}'_i{}^{\mu e} \widetilde{Y}'_i{}^{ee} \widetilde{Y}'_j{}^{\mu e} \widetilde{Y}'_j{}^{ee}}{m_{A_i}^2 m_{A_j}^2} + \frac{\widetilde{Y}'_i{}^{e\mu} \widetilde{Y}'_i{}^{ee} \widetilde{Y}'_j{}^{e\mu} \widetilde{Y}'_j{}^{ee}}{m_{A_i}^2 m_{A_j}^2} \right) \left. \right]. \quad (4.47) \end{aligned}$$

The first two addends are the contributions solely from the doubly charged decay channel for either the left or the right triplets, the first double sum is the contribution from the scalar neutral decay channel and the last double sum from pseudoscalar decay channel. Note, that Interference between either of these channels vanishes.

And with this, it appears rather simple to compute the branching ratio ( $BR$ ) for the  $\mu \rightarrow 3e$  decay in the following way:

$$BR = \frac{\Gamma}{\Gamma_{tot}}, \quad (4.48)$$

with  $\Gamma_{tot}$  as the total decay width. And so, the final form is

$$\begin{aligned} BR = & \frac{m_\mu^5}{3 \cdot 2^{12} \pi^2 \cdot \Gamma_{tot}} \left[ \left( \frac{Y_L^{e\mu} Y_L^{ee}}{m_L^{-2}} \right)^2 + \left( \frac{Y_R^{\mu e} Y_R^{ee}}{m_R^{-2}} \right)^2 \right. \\ & + 2 \sum_{i=1}^4 \sum_{j=1}^4 \left( \frac{\tilde{Y}_i^{e\mu} \tilde{Y}_i^{ee} \tilde{Y}_j^{e\mu} \tilde{Y}_j^{ee}}{m_i^2 m_j^2} + \frac{\tilde{Y}_i^{\mu e} \tilde{Y}_i^{ee} \tilde{Y}_j^{\mu e} \tilde{Y}_j^{ee}}{m_i^2 m_j^2} \right) \\ & \left. + 2 \sum_{i=1}^2 \sum_{j=1}^2 \left( \frac{\tilde{Y}'_i{}^{\mu e} \tilde{Y}'_i{}^{ee} \tilde{Y}'_j{}^{\mu e} \tilde{Y}'_j{}^{ee}}{m_{A_i}^2 m_{A_j}^2} + \frac{\tilde{Y}'_i{}^{e\mu} \tilde{Y}'_i{}^{ee} \tilde{Y}'_j{}^{e\mu} \tilde{Y}'_j{}^{ee}}{m_{A_i}^2 m_{A_j}^2} \right) \right]. \quad (4.49) \end{aligned}$$

$BR$  is now written as a function of the bidoublet and triplet Yukawa couplings.



## 5. Connection To Neutrino Physics

Now that the branching ratio for the  $\mu \rightarrow 3e$  process has been obtained, the next step is to take neutrino physics into account. Slightly rearranging eq. (3.17) back from Chapter 3, one ends up with:

$$M = \begin{pmatrix} \alpha Y_R \nu_R & m_D \\ m_D & Y_R \nu_R \end{pmatrix}, \quad (5.1)$$

with  $\alpha = \frac{\nu_L}{\nu_R}$ . Furthermore, in the course of this thesis, the assumption  $Y_L = Y_R$  has been made. With the given results for the *PMNS* Matrix and the observed  $\nu$  masses (see Ref. [9]), the flavour diagonal mass matrix  $m_\nu$  can be computed. In the course of this computation, a value for  $m_1 = m_2/100$  has been assumed in order to avoid numeric hiccups that might arise for  $m_1 = 0$ , as well as a normal hierarchy with  $m_1 < m_2 < m_3$ . Additionally, both the *CP* violation and the Majorana Phases have been set to zero for this calculation.

$$m_\nu = U_{PMNS} \cdot \text{diag}(m_1, m_2, m_3) \cdot (U_{PMNS})^T.$$

In order to determine the requested Coupling  $Y_R$

$$\begin{aligned} m_\nu &= \alpha Y_R \nu_R - m_D (Y_R \nu_R)^{-1} m_D \\ \Rightarrow m_D^{-1/2} m_\nu m_D^{-1/2} &= \alpha m_D^{-1/2} Y_R \nu_R m_D^{-1/2} - m_D^{1/2} (Y_R \nu_R)^{-1} m_D^{1/2}. \end{aligned}$$

This equation is (according to Ref. [12]) of the form

$$B = \alpha A - A^{-1},$$

and with  $R$  as the diagonalization matrix that diagonalizes both A and B yields:

$$\begin{aligned} \Rightarrow B &= R B_D R^{-1} \\ A &= R A_D R^{-1} \\ \Leftrightarrow A^{-1} &= R A_D^{-1} R^{-1} \\ \Rightarrow R B_D R^{-1} &= R(\alpha A_D - A_D^{-1}) R^{-1} \\ \Leftrightarrow B_D &= (\alpha A_D - A_D^{-1}). \end{aligned}$$

Note that this is a quadratic equation that provides 8 different solutions for  $A_D$ , as every dimension yields two possible solutions. The different solutions for  $A_D$  have the following

## 5. Connection To Neutrino Physics

---

signs for their eigenvalues:

$$\begin{aligned}
 A_{D1} &\rightarrow \begin{pmatrix} + \\ + \\ + \end{pmatrix}, & A_{D2} &\rightarrow \begin{pmatrix} + \\ + \\ - \end{pmatrix}, & A_{D3} &\rightarrow \begin{pmatrix} + \\ - \\ + \end{pmatrix}, & A_{D4} &\rightarrow \begin{pmatrix} + \\ - \\ - \end{pmatrix}, \\
 A_{D5} &\rightarrow \begin{pmatrix} - \\ + \\ + \end{pmatrix}, & A_{D6} &\rightarrow \begin{pmatrix} - \\ + \\ - \end{pmatrix}, & A_{D7} &\rightarrow \begin{pmatrix} - \\ - \\ + \end{pmatrix}, & A_{D8} &\rightarrow \begin{pmatrix} - \\ - \\ - \end{pmatrix}.
 \end{aligned}$$

It is worthwhile to take a closer look at these Eigenvalues, as it appears that the solutions 1-4 have the exact opposite signs from solutions 5-8, even if in a deviant order. Keep in mind though, that a these Eigenvalues do not necessarily have the same modulus, but are only identical in three to four significant digits. Within the scope of this computation, however, this turns out to be irrelevant. As a consequence, these solutions can be regarded as just having an overall phase factor of  $-1$ , which is from a quantum mechanics point-of-view exactly the same, meaning that only 4 solutions need be computed.

These diagonal matrices  $A_D$  can now be transferred to the desired Triplet Yukawa Coupling  $Y_R$

$$\begin{aligned}
 \Rightarrow Y_R v_R &= m_D^{1/2} A m_D^{1/2} \\
 &= m_D^{1/2} R A_D R^{-1} m_D^{1/2}.
 \end{aligned} \tag{5.2}$$

Inserting this value for the triplet coupling into eq. (4.1) and (4.40) yields the different Yukawas in the neutral scalar and pseudoscalar channel, respectively. Now that the triplet coupling  $Y_R$  is expressed as a function of  $m_D$ , which in turn is a function of the bidoublet Yukawas  $Y_1$  and  $Y_2$ ,  $BR$  is also expressed as a function of the bidoublet Yukawas. Furthermore, as the charged lepton masses

$$m_L = \frac{1}{\sqrt{2}} (v_1 Y_1 + v_2 Y_2)$$

are known,  $Y_2$  is dependent of  $Y_1$  and thus only one bidoublet Yukawa coupling remains as an input for  $BR$ . However, the VEVs are still an issue, yet they as well may be constrained. As the mass of the  $W$ -Boson obeys the condition (See Ref. [3])

$$m_W = \frac{g_2}{2} \sqrt{v_1^2 + v_2^2}, \tag{5.3}$$

where  $g_2$  is the gauge coupling,  $v_1$  and  $v_2$  can be expressed as

$$\tan \beta = \frac{v_1}{v_2}. \tag{5.4}$$

---

These VEVs can be parametrized as:

$$v_1 = \tan \beta \cdot v_2 \quad (5.5)$$

$$v_2 = \frac{2m_W}{g_2 \sqrt{1 + \tan^2 \beta}}. \quad (5.6)$$

Thus, by the bidoublet Yukawa  $Y_1$  and  $\tan \beta$  alone,  $BR$  can be computed. Finally, only one more assumption has been made and that is  $Y_1$  and  $Y_2$  are diagonal matrices.

$$Y_1 = \text{diag} (Y_{111}, Y_{122}, Y_{133}). \quad (5.7)$$

So,  $BR$  turns out to be depending on four parameters:  $\tan \beta, Y_{111}, Y_{122}$  and  $Y_{133}$ .

$$\begin{aligned}
BR = & \frac{m_\mu^5}{3 \cdot 2^{12} \pi^2 \cdot \Gamma_{tot}} \left[ \left( \left( \frac{1}{m_L^{-4}} \right) + \left( \frac{1}{m_R^{-4}} \right) \right) \right. \\
& \cdot (Y_R^{e\mu}(\tan \beta, Y_{111}, Y_{122}, Y_{133}) Y_R^{ee}(\tan \beta, Y_{111}, Y_{122}, Y_{133}))^2 \\
& + 2 \sum_{i=1}^4 \sum_{j=1}^4 \left( \frac{\tilde{Y}_i^{e\mu}(\tan \beta, Y_{111}, Y_{122}, Y_{133}) \tilde{Y}_i^{ee}(\tan \beta, Y_{111}, Y_{122}, Y_{133})}{m_i^2 m_j^2} \right. \\
& \quad \cdot \frac{\tilde{Y}_j^{e\mu}(\tan \beta, Y_{111}, Y_{122}, Y_{133}) \tilde{Y}_j^{ee}(\tan \beta, Y_{111}, Y_{122}, Y_{133})}{m_i^2 m_j^2} \\
& + \frac{\tilde{Y}_i^{\mu e}(\tan \beta, Y_{111}, Y_{122}, Y_{133}) \tilde{Y}_i^{ee}(\tan \beta, Y_{111}, Y_{122}, Y_{133})}{m_i^2 m_j^2} \\
& \quad \left. \cdot \frac{\tilde{Y}_j^{\mu e}(\tan \beta, Y_{111}, Y_{122}, Y_{133}) \tilde{Y}_j^{ee}(\tan \beta, Y_{111}, Y_{122}, Y_{133})}{m_{A_i}^2 m_{A_j}^2} \right) \\
& + 2 \sum_{i=1}^4 \sum_{j=1}^4 \left( \frac{\tilde{Y}'_i^{e\mu}(\tan \beta, Y_{111}, Y_{122}, Y_{133}) \tilde{Y}'_i^{ee}(\tan \beta, Y_{111}, Y_{122}, Y_{133})}{m_{A_i}^2 m_{A_j}^2} \right. \\
& \quad \cdot \frac{\tilde{Y}'_j^{e\mu}(\tan \beta, Y_{111}, Y_{122}, Y_{133}) \tilde{Y}'_j^{ee}(\tan \beta, Y_{111}, Y_{122}, Y_{133})}{m_{A_i}^2 m_{A_j}^2} \\
& + \frac{\tilde{Y}'_i^{\mu e}(\tan \beta, Y_{111}, Y_{122}, Y_{133}) \tilde{Y}'_i^{ee}(\tan \beta, Y_{111}, Y_{122}, Y_{133})}{m_{A_i}^2 m_{A_j}^2} \\
& \quad \left. \left. \cdot \frac{\tilde{Y}'_j^{\mu e}(\tan \beta, Y_{111}, Y_{122}, Y_{133}) \tilde{Y}'_j^{ee}(\tan \beta, Y_{111}, Y_{122}, Y_{133})}{m_{A_i}^2 m_{A_j}^2} \right) \right]. \quad (5.8)
\end{aligned}$$

All other model parameters can be found in the appendix [A.1](#).



## 6. Discussion

With this algorithm, it is possible to derive contourplots for different values of  $\tan\beta$  with fixed input-values for any one of the three couplings  $Y_{111}, Y_{122}, Y_{133}$ . These plots can then be used to determine which regions of the phase space can be rejected, as the branching ratio would be too high for the  $\mu \rightarrow 3e$  decay channel. In the following figures, the regions of accepted data will be displayed in dark blue colours, and the rejected regions in red and yellow colours. Note that the axes do not denote the values of the couplings  $Y_{111}, Y_{122}$  or  $Y_{133}$  but their logarithms  $\log_{10}[Y_{111}]$  etc.. Also the contours display  $\log_{10}[BR]$  instead of the branching ratio in its original state.

The experimental bound for this decay is  $BR < 10^{-12}$  [9] and will be the threshold for the accepted dataset and displayed as a red line in the following plots. The range for the Yukawas was  $[10^{-9}, 10^{-2}]$  for the whole dataset.

### 6.1. First Solution

The first solution with only positive Eigenvalues for the triplet Yukawas gives the following results for different values of  $\tan\beta$ .

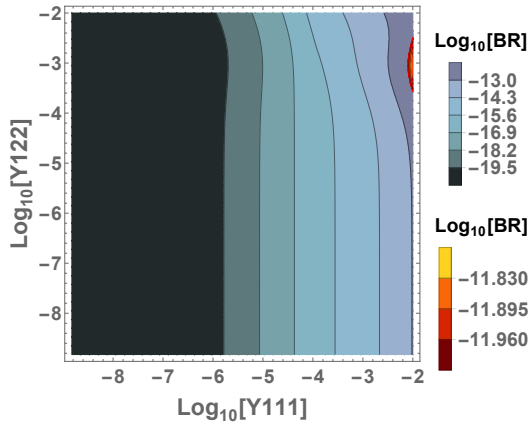
#### Fixed $Y_{133}$

Comparing figures 6.1a, 6.1b and 6.1c only results in a slightly larger region of rejection, as well as a rather tiny new region at about  $Y_{111} = Y_{122} = 10^{-2}$  for  $\tan\beta = 0.5$ . Apart from that, no huge differences can be encountered for values between  $\tan\beta = 0.1$  and  $\tan\beta = 0.9$ , in this dataset.

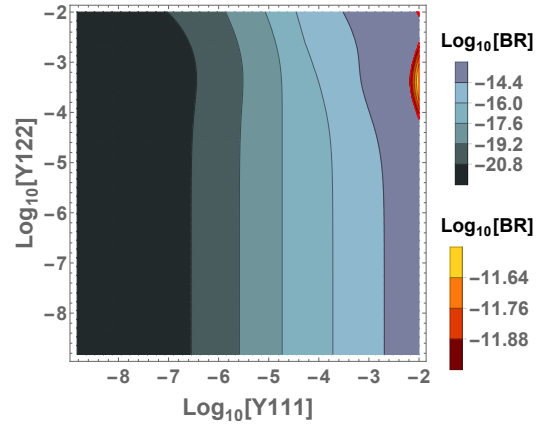
For the values  $\tan\beta > 1$  the regions of rejection drastically increase in size. For  $\tan\beta = 1.1$  this region starts with values of  $Y_{111} \geq 10^{-5.1}$  for almost all values of  $Y_{122}$ , except for  $Y_{122} \approx 10^{-2.2}$  where this region is slightly narrowed. Also, for  $Y_{111} \leq 10^{-5.5}$  and  $Y_{122} \geq 10^{-2.2}$ , another small region of rejection appears. For larger values of  $\tan\beta$ , these two regions increase in size and almost cut the accepted region in two pieces for  $\tan\beta = 10$ , forming a bottleneck at around  $Y_{111} = 10^{-5.5}$  and  $Y_{122} = 10^{-3.8}$ .

Note, that the plotted region grows slightly smaller for  $\tan\beta > 1$ . Starting with figure 6.1d, the top right corner in the plot features a white space, growing larger with increasing  $\tan\beta$ . Additionally, in figure 6.1f ( $\tan\beta = 10$ ) for example, the plotted region has its limits for the abscissa at about  $Y_{111} = 10^{-2.9}$ , as well as for the ordinate at  $Y_{122} = 10^{-2.5}$ . These regions feature complex-valued results for the couplings. Since before in chapter 4 the limit of only real couplings has been set, technically, these values exceed the domain of  $\Gamma$ . Hence, with the form from Chapter 4, as  $Y_R \in \mathbb{C}$ , no sensible result for  $BR$  can

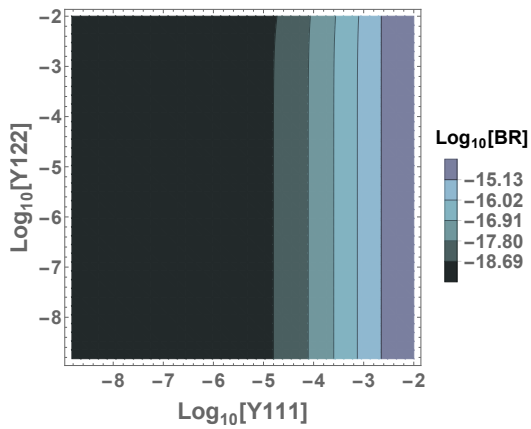
6. Discussion



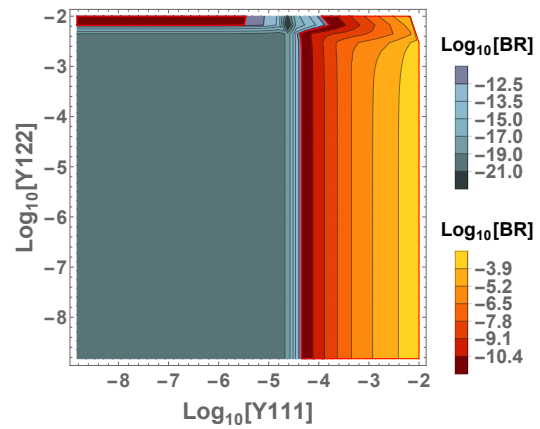
(a) Contourplot with  $\tan \beta = 0.1$ .



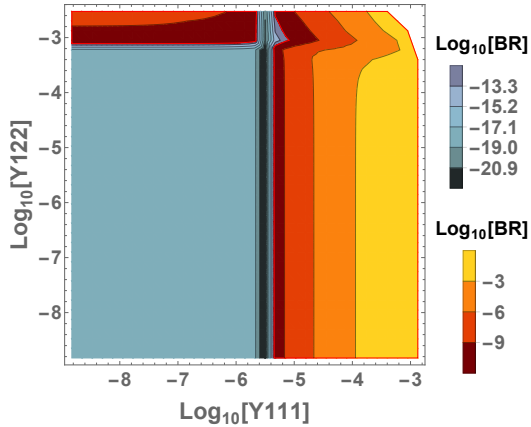
(b) Contourplot with  $\tan \beta = 0.5$ .



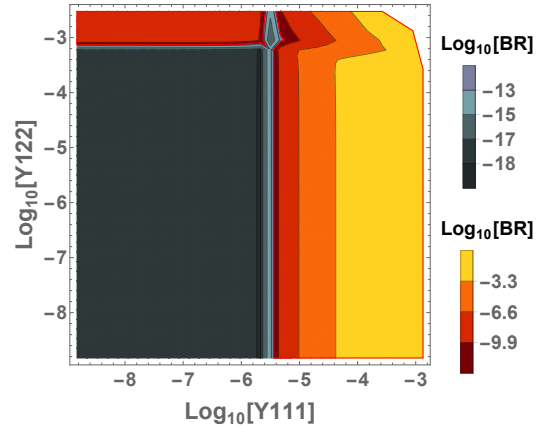
(c) Contourplot with  $\tan \beta = 0.9$ .



(d) Contourplot with  $\tan \beta = 1.1$ .

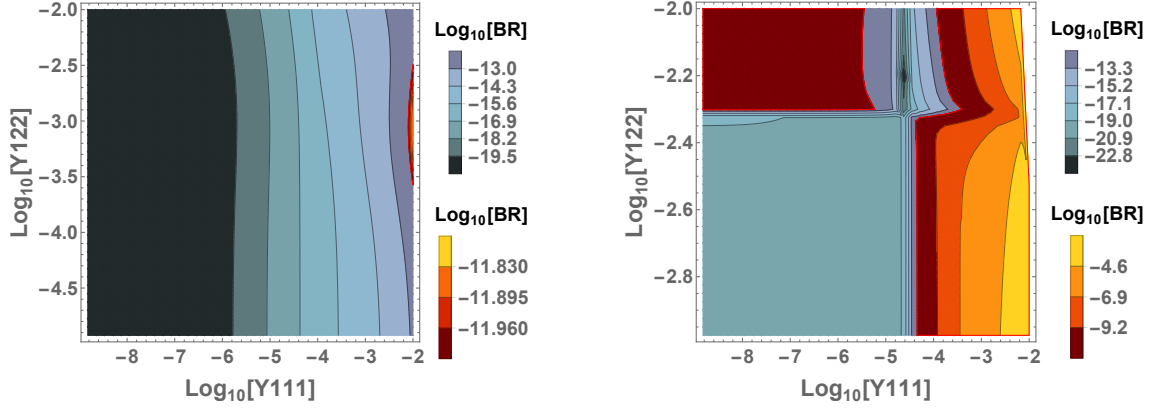


(e) Contourplot with  $\tan \beta = 5$ .

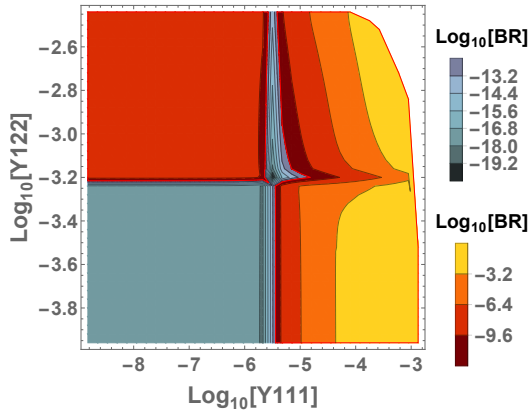


(f) Contourplot with  $\tan \beta = 10$ .

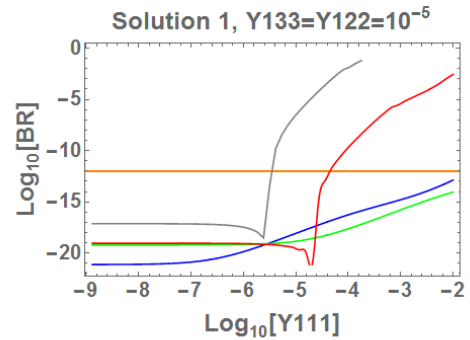
Figure 6.1.. First solution: In all of the plots above  $Y_{133} = 10^{-5}$  is a fixed value. The axes show  $\log_{10} [Y_{111}]$  and  $\log_{10} [Y_{122}]$  and the contours denote values of  $\log_{10} [BR]$  as well. The dark blue colours indicate accepted regions within the parameter space while the red and yellow colours indicate rejected regions. The red border contour outlines the values for  $BR = 10^{-12}$ . Note the slightly larger region of rejection in 6.1b as well as the rather small region of rejection in the top right corner, whereas the whole of figure 6.1c is accepted. Figures 6.1d, 6.1e and 6.1f each display two separate regions of rejection increasing in size. Additionally, in these three figures, the plotted region grows smaller in size, as the values for  $Y_{111}$  and  $Y_{122}$  exceed the domain of  $BR$ .



(a) Contourplot with  $\tan\beta = 0.1$ . The part displaying dependence of  $Y_{122}$  has been zoomed in. (b) Contourplot with  $\tan\beta = 1.1$ . The part displaying dependence of  $Y_{122}$  has been zoomed in.



(c) Contourplot with  $\tan\beta = 10$ . The part displaying dependence of  $Y_{122}$  has been zoomed in.



—  $\tan\beta=0.1$  —  $\tan\beta=0.9$  —  $\tan\beta=1.1$  —  $\tan\beta=10$

(d) Plot for  $\log_{10}[BR]$  as a function of  $\log_{10}[Y_{111}]$ . Both  $Y_{133}$  and  $Y_{122}$  are constant at  $10^{-5}$  for different values of  $\tan\beta$ . The orange line indicating  $BR = 10^{-12}$  separates the accepted from the rejected region of the parameter space.

Figure 6.2.. First solution: In all of the plots above  $Y_{133} = 10^{-5}$  is a fixed value, yet in contrast to figure 6.1, certain parts of the plots have been zoomed in. In figure 6.2d, various values of  $\tan\beta$  have been used to compute  $BR$  with both  $Y_{122}$  and  $Y_{133}$  given a constant value.

## 6. Discussion

---

be given and another form, including complex-valued couplings, is required. However, as can for example be seen in figure 6.2c, the part that exceeds the domain is rejected already. Implementing a formula for  $BR$  with  $Y_R \in \mathbb{C}$  therefore appears to be redundant.

As there are no fundamental changes happening between  $\tan \beta = 0.1$  and  $\tan \beta = 0.9$  as well as between  $\tan \beta = 1.1$  and  $\tan \beta = 10$ , these plots will be left out in the following discussion. However, the plots not featured in this chapter can be found in the Appendix. Moreover, since some plots feature large parts, where  $BR$  is more or less independent of one parameter, in the following, parts of the parameter space that do not exhibit dependence of both plotted variables will be broken down to one-dimensional curves and the regions that do exhibit dependence of both variables will be magnified.

### Fixed $Y_{122}$

The plots in figure 6.3 show the  $\log_{10} [BR]$  for a fixed value of  $Y_{122} = 10^{-5}$  as well as a function of  $Y_{111}$  and  $Y_{133}$ .

For  $0.1 < \tan \beta < 0.9$  no region is rejected in this dataset as  $BR$  lies well below  $10^{-12}$ . However, for  $1.1 < \tan \beta < 10$  a region of rejection starts at about the same value as in figures 6.1d and 6.1f. Yet, these appear to be independent of  $Y_{133}$ . Also, like for a fixed  $Y_{111}$  in figure 6.1, for values of  $Y_{111} > 10^{-2.9}$  and  $\tan \beta = 10$  the domain is exceeded. Note that the case of  $Y_{122} = \text{const.}$  also features parts that are independent of one variable. Setting  $Y_{133}$  to a constant value does not give a different result than figure 6.2d, which is why there is no such plot.

### Fixed $Y_{111}$

For a fixed value of  $Y_{111} = 10^{-7}$ , as well as variable  $Y_{122}$  and  $Y_{133}$ , for the same four values of  $\tan \beta$  as shown in figure 6.3, can be seen in figure 6.5.

For values of  $\tan \beta \leq 0.9$ , all points of the parameter space lie well within the bounds. Only for  $\tan \beta \geq 1.1$  regions of rejection appear, which are independent of  $Y_{133}$  and start at the same values of  $Y_{122}$  as they did in figure 6.1d or 6.1f, respectively. Similarly, for the same values as for  $Y_{122}$  in figure 6.1, the domain is exceeded.

In total, for  $Y_R$  being a positive definite matrix, it is save to say, that  $Y_{133}$  has little to no impact on  $BR$  and thus cannot be constrained. However,  $Y_{111}$  and  $Y_{122}$  can be constrained. Readout values for the minimal and maximal rejected region that can be found in the Appendix. As a rule of thumb, it can be observed in figures 6.2d and 6.6d:

$$\begin{aligned} Y_{111_{max}} &\in ]10^{-5.6}, 10^{-4.6} [ \\ Y_{122_{max}} &\in ]10^{-3.2}, 10^{-2.2} [ . \end{aligned}$$

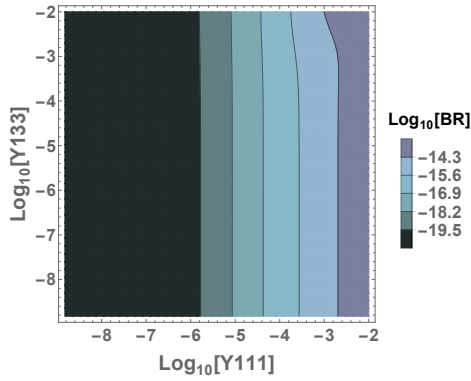
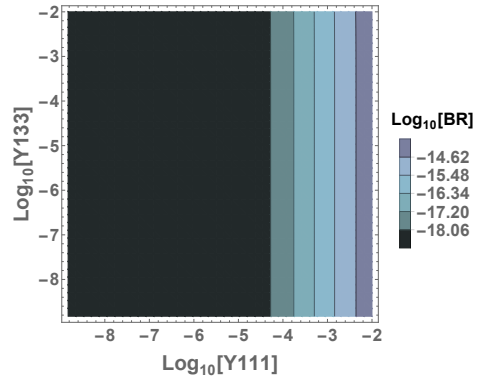
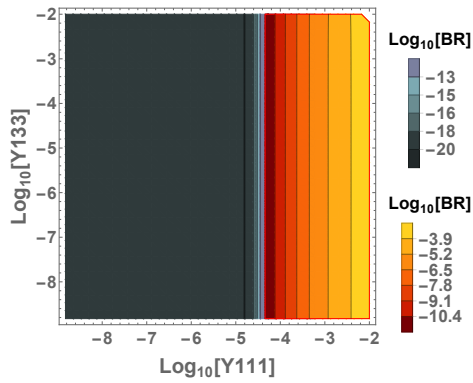
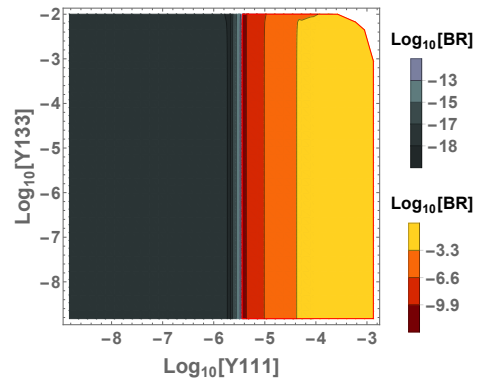
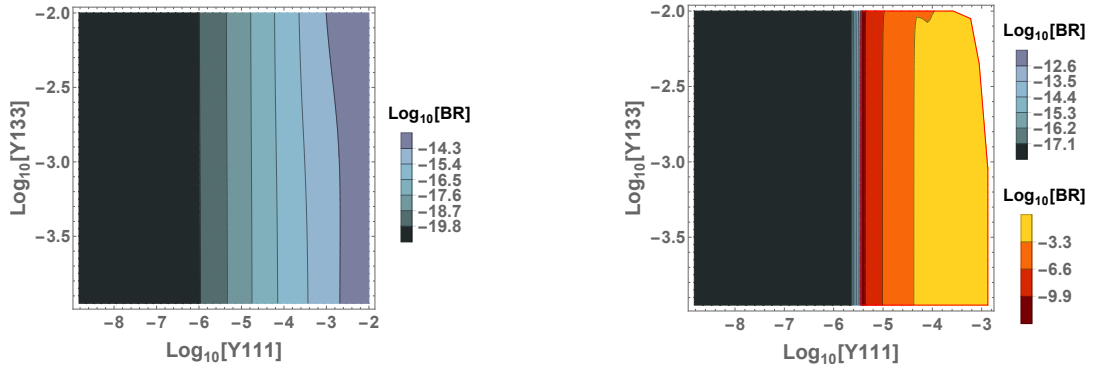
(a) Contourplot with  $\tan \beta = 0.1$ .(b) Contourplot with  $\tan \beta = 0.9$ .(c) Contourplot with  $\tan \beta = 1.1$ .(d) Contourplot with  $\tan \beta = 10$ .

Figure 6.3.. First solution: In all four plots  $Y_{122} = 10^{-5}$  is a fixed value. The  $x$ -axis and the colouring are the same as in figure 6.1, yet the  $y$ -axis denotes  $\log_{10} [Y_{133}]$ . As in figures 6.3a and 6.3b only dark blue colours are shown, no parts of the parameter space are rejected. Yet in figure 6.3c a region of rejection starts at about  $Y_{111} = 10^{-4.8}$ . In 6.3d rejection starts at about  $Y_{111} = 10^{-5.6}$ . Also, white regions appear in both plots at the top right, where Yukawas exceed domain.

## 6. Discussion



- (a) Contourplot with  $\tan\beta = 0.1$ . The part displaying dependence of  $Y133$  has been zoomed in. (b) Contourplot with  $\tan\beta = 1.1$ . The part displaying dependence of  $Y133$  has been zoomed in.

Figure 6.4.. First solution: Both plots have the same fixed value of  $Y122 = 10^{-5}$  and the parts showing dependence of  $Y133$  are zoomed in, similarly to figure 6.2. Note that setting  $Y133 = \text{const.}$  for parts independent of  $Y133$  does not yield a different Plot than figure 6.2d.

## 6.2. Second Solution

### Fixed $Y133$

The second solution where the first two Eigenvalues of the triplet Yukawas are positive, while the third one is negative, give the following results for the branching ratio. Figure 6.7 displays contourplots for  $\log_{10}[BR]$  as a function of  $Y111$  and  $Y122$  with  $Y133 = 10^{-5}$  fixed at the same value as in figure 6.1.

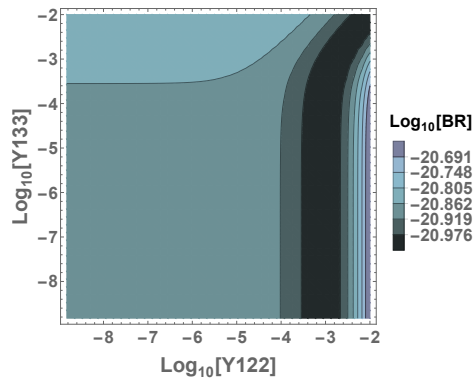
### Fixed $Y122$

The plots in figure 6.8 show the  $\log_{10}[BR]$  for a fixed value of  $Y122 = 10^{-5}$  as a function of  $Y111$  and  $Y133$  just like in figure 6.3.

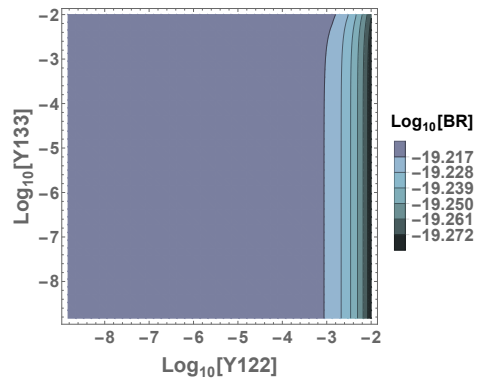
### Fixed $Y111$

The plots in figure 6.9 show the  $\log_{10}[BR]$  for a fixed value of  $Y111 = 10^{-7}$  as well as a function of  $Y122$  and  $Y133$ . similarly to figure 6.5.

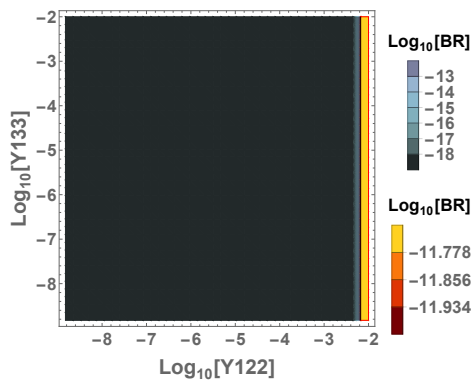
As in the section before, precise parameters drawn from the figures can be found in the Appendix. But some features worth discussing may be observed here. The dependence of  $Y133$  appears higher for this solution than in the positive definite case, even tough figures 6.8 and 6.9 displays rather large regions where  $BR$  is either independent of  $Y133$  or does not even approach the threshold of  $BR = 10^{-12}$ .



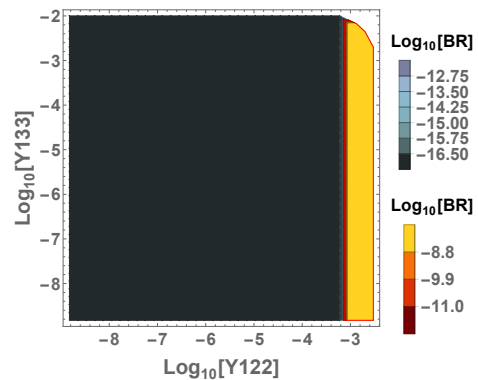
(a) Contourplot with  $\tan \beta = 0.1$ .



(b) Contourplot with  $\tan \beta = 0.9$ .

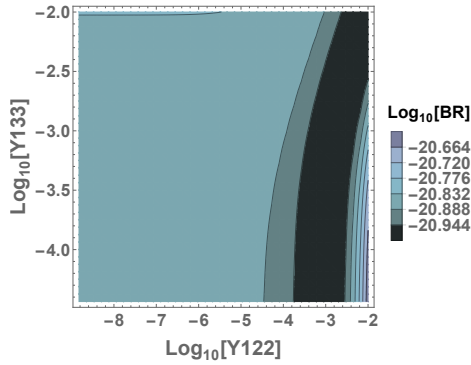


(c) Contourplot with  $\tan \beta = 1.1$ .

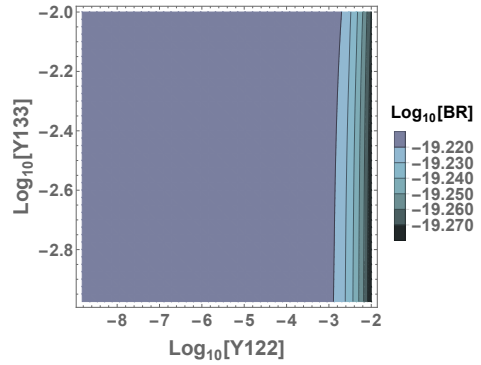


(d) Contourplot with  $\tan \beta = 10$ .

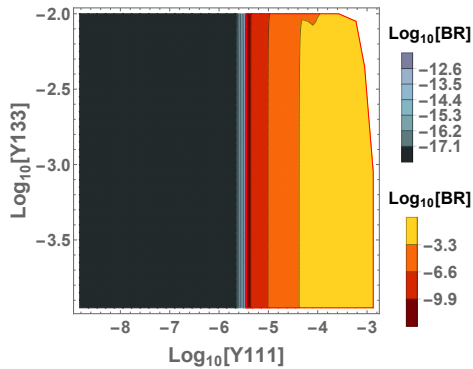
Figure 6.5.. First solution: In all four plots  $Y_{133} = 10^{-5}$  is a fixed value. The  $x$ -axis denotes  $\log_{10}[Y_{122}]$  and the  $y$ -axis denotes  $\log_{10}[Y_{122}]$ . The colouring is the same as in the figures from before.



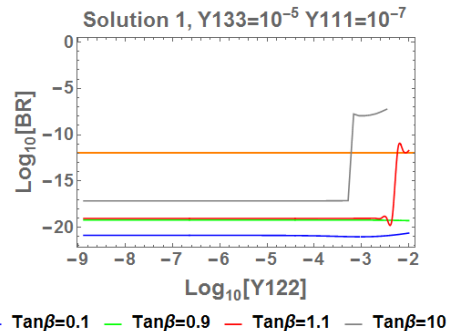
(a) Contourplot with  $\tan\beta = 0.1$ . The part displaying dependence of  $Y133$  has been zoomed in.



(b) Contourplot with  $\tan\beta = 0.9$ . The part displaying dependence of  $Y133$  has been zoomed in.

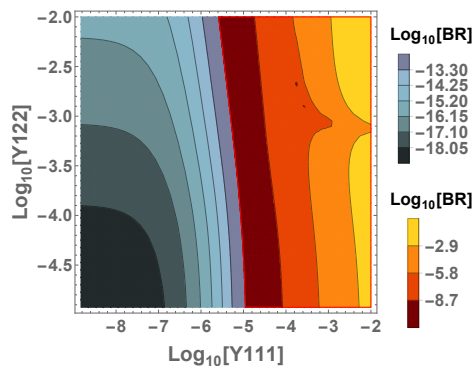


(c) Contourplot with  $\tan\beta = 1.1$ . The part displaying dependence of  $Y133$  has been zoomed in.

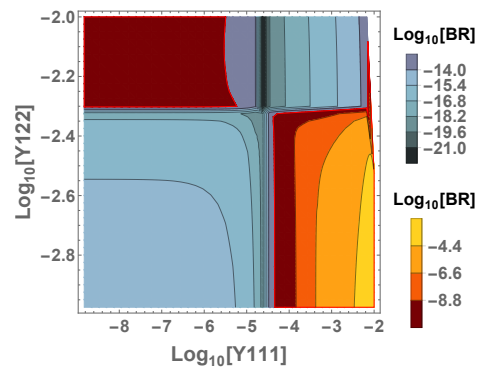


(d) Plot for  $\log_{10}[BR]$  as a function of  $\log_{10}[Y122]$ .  $Y111 = 10^{-7}$  and  $Y133 = 10^{-5}$  are constant. For different values of  $\tan\beta$ . The orange line indicating  $BR = 10^{-12}$  separates the accepted from the rejected region of the parameter space.

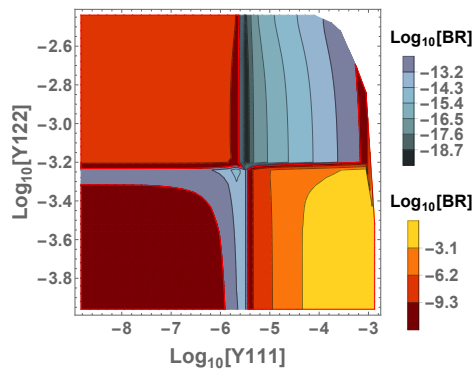
Figure 6.6.. First solution: In all of the plots above  $Y111 = 10^{-7}$  is a fixed value, yet in contrast to figure 6.1, certain parts of the plots have been zoomed in. In figure 6.2d, various values of  $\tan\beta$  have been used to compute  $BR$  with both  $Y122$  and  $Y133$  given a constant value.



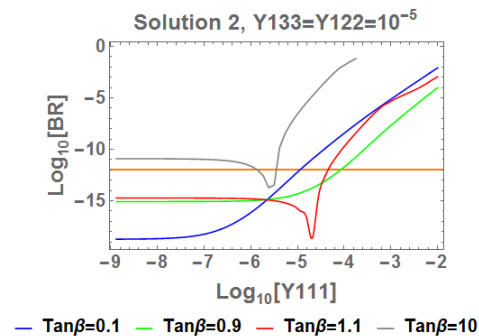
(a) Contourplot with  $\tan \beta = 0.1$ .



(b) Contourplot with  $\tan \beta = 1.1$ .

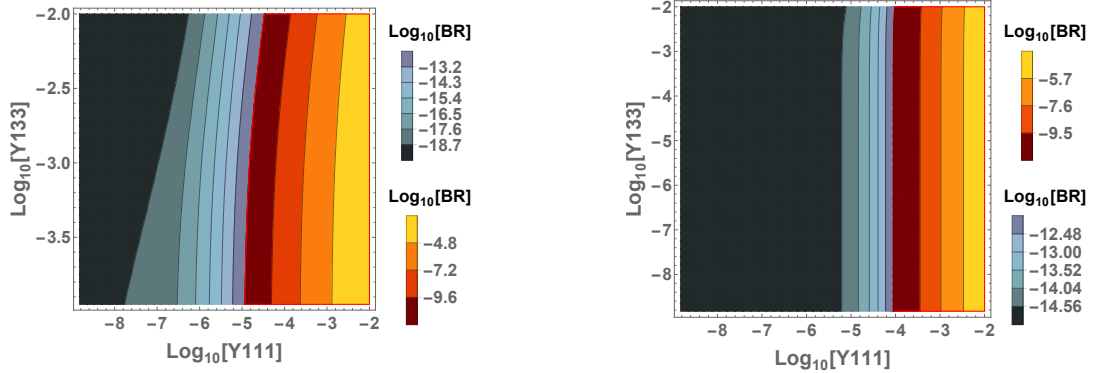


(c) Contourplot with  $\tan \beta = 10$ .



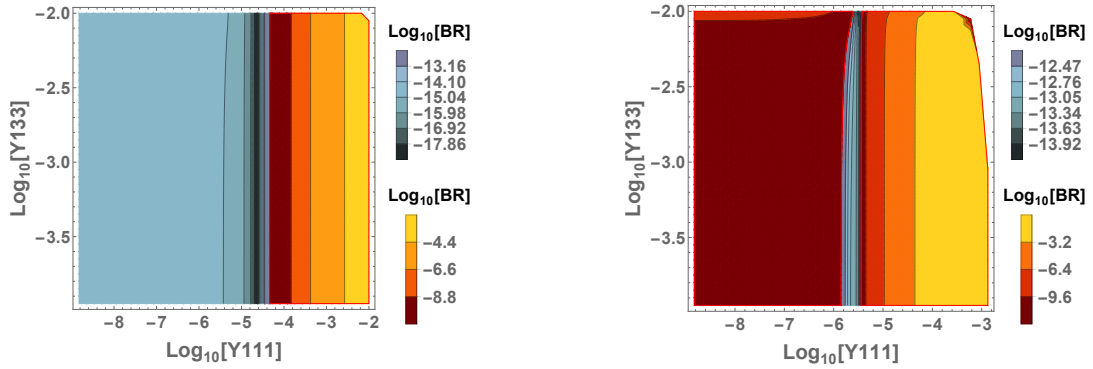
(d) Multiple curves for different values of  $\tan \beta$  with  $Y_{133}$  and  $Y_{122}$  as a fixed value once more. The orange line divides the dataset in accepted and rejected regions.

Figure 6.7.. Second solution: Axes and colouring display the same as in figure 6.1, also again  $Y_{133} = 10^{-5}$  as a fixed value. Parts that appear to be independent of  $Y_{122}$  have been magnified and a plot featuring different curves of  $BR$  similar to 6.2d has been added.



(a) Contourplot with  $\tan \beta = 0.1$ .

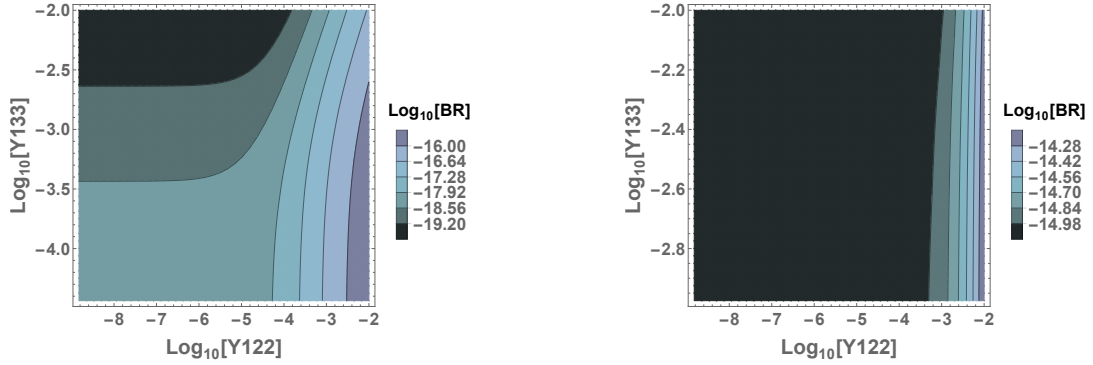
(b) Contourplot with  $\tan \beta = 0.9$ .



(c) Contourplot with  $\tan \beta = 1.1$ .

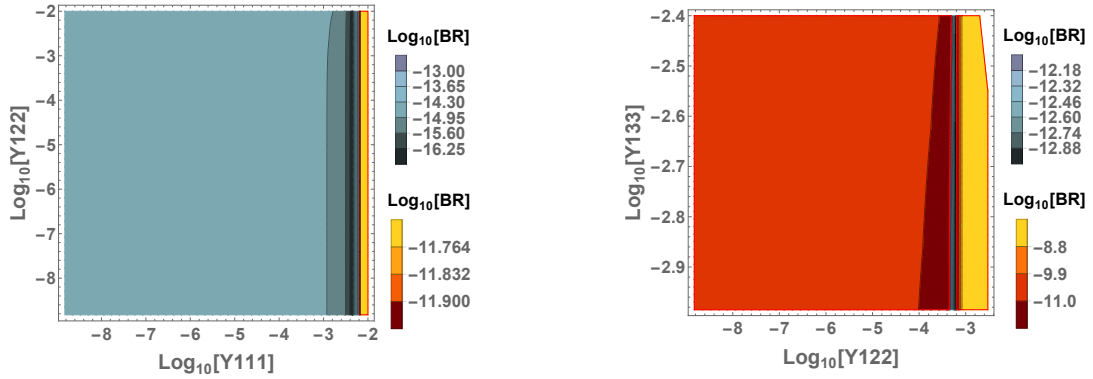
(d) Contourplot with  $\tan \beta = 10$ .

Figure 6.8.. Second solution: In both plots  $Y_{122} = 10^{-5}$  is a fixed value. Axes and colouring display the same as in figure. Regions independent of  $Y_{133}$  have been magnified. 6.3.



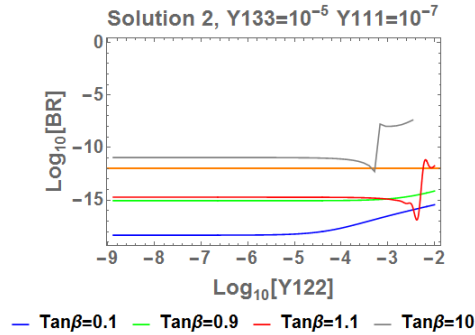
(a) Contourplot with  $\tan \beta = 0.1$ .

(b) Contourplot with  $\tan \beta = 0.9$ .



(c) Contourplot with  $\tan \beta = 1.1$ .

(d) Contourplot with  $\tan \beta = 5$ .



(e) Like before, several values of  $\tan \beta$  were used to compute  $\log_{10}[BR]$  as a function of  $\log_{10}[Y122]$ . The orange horizontal line denotes  $BR = 10^{-12}$ .

Figure 6.9.. Second solution: In all plots  $Y111 = 10^{-7}$  is a fixed value. Axes and colouring are analogous to figure 6.3 .

### 6.3. Third Solution

The third solution where the first two Eigenvalues of the triplet Yukawas are positive, while the third one is negative, give the following results:

#### Fixed $Y_{133}$

Figure 6.10 displays contour plots for  $\log_{10}[BR]$  as a function of  $Y_{111}$  and  $Y_{122}$  with  $Y_{133} = 10^{-5}$  fixed at the same value as in figure 6.1.

#### Fixed $Y_{122}$

The plots in figure 6.11 show the  $\log_{10}[BR]$  for a fixed value of  $Y_{122} = 10^{-5}$  as a function of  $Y_{111}$  and  $Y_{133}$  just like in figure 6.3.

#### Fixed $Y_{111}$

The plots in figure 6.12 show the  $\log_{10}[BR]$  for a fixed value of  $Y_{111} = 10^{-7}$  as a function of  $Y_{122}$  and  $Y_{133}$  just like in figure 6.5.

Again, the branching ratio for the third solution of  $Y_R$  is for a wide array of parameters independent of  $Y_{133}$ . It is also noteworthy that a "bubble" can be found in figure 6.10a at  $\log_{10}[Y_{111}] = -4.8$  and  $\log_{10}[Y_{122}] = -4.4$ . Additionally two other bubbles can be found in its vicinity. Detailed numbers can be found in the appendix. Apart from that, concise form of constraints can be obtained, for  $\tan\beta < 1$ ,  $BR(Y_{111})$  seems to be monotonously increasing, apart from a few valleys. But – especially when regarding figure 6.11d – no clear rule for their behaviour can be found for other cases.

### 6.4. Fourth Solution

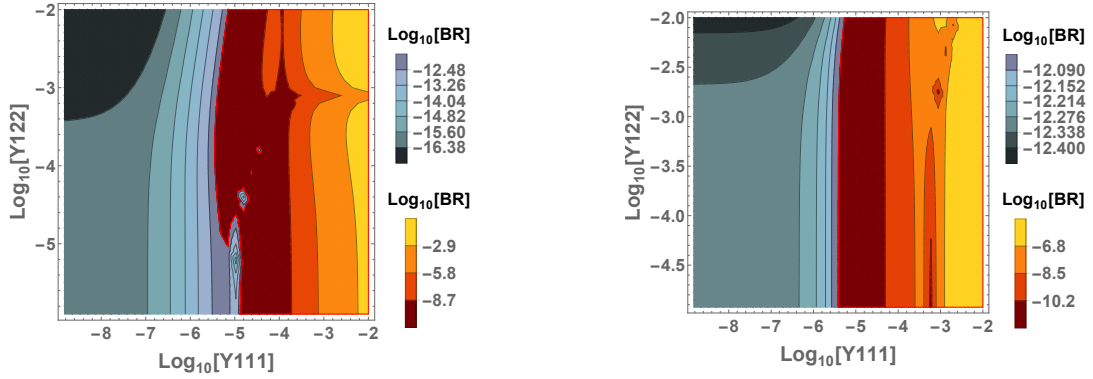
The fourth solution, where the first two Eigenvalues of the triplet Yukawas are positive, while the third one is negative, show the following results:

#### Fixed $Y_{133}$

Figure 6.13 displays contour plots for  $\log_{10}[BR]$  as a function of  $Y_{111}$  and  $Y_{122}$  with  $Y_{133} = 10^{-5}$  fixed at the same value as in figure 6.1.

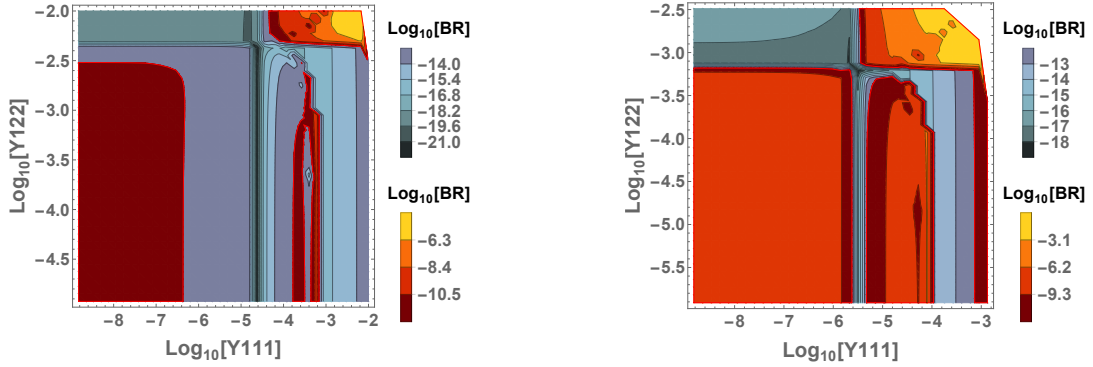
#### Fixed $Y_{122}$

The plots in figure 6.14 show the  $\log_{10}[BR]$  for a fixed value of  $Y_{122} = 10^{-5}$  as a function of  $Y_{111}$  and  $Y_{133}$  just like in figure 6.3.



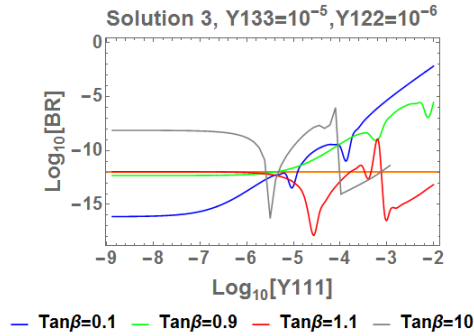
(a) Contourplot with  $\tan \beta = 0.1$ .

(b) Contourplot with  $\tan \beta = 0.9$ .



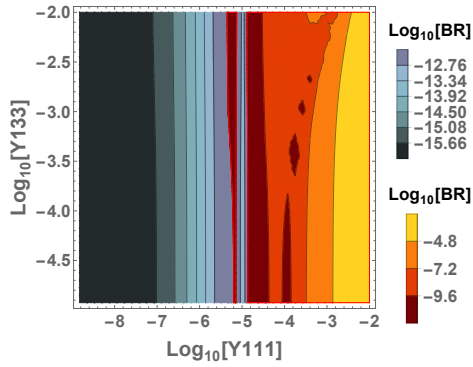
(c) Contourplot with  $\tan \beta = 1.1$ .

(d) Contourplot with  $\tan \beta = 10$ .

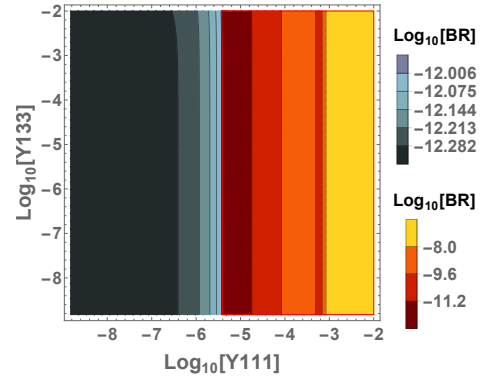


(e) Multiple curves for different values of  $\tan \beta$  at fixed  $Y_{133} = 10^{-5}$  and  $Y_{122} = 10^{-6}$ . The orange line divides the dataset in accepted and rejected regions.

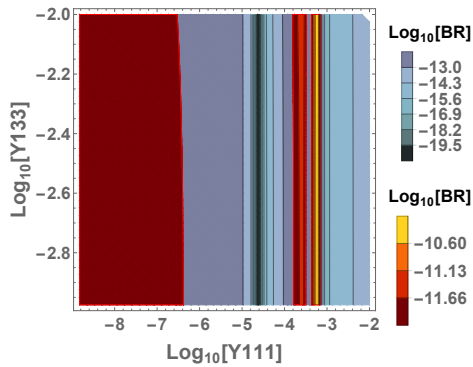
Figure 6.10.. Third solution: Axes and colouring display the same as in figure 6.1, also again  $Y_{133} = 10^{-5}$  as a fixed value. Parts that appear to be independent of  $Y_{122}$  have been magnified and a plot featuring different curves of  $BR$  similar to 6.2d has been added.



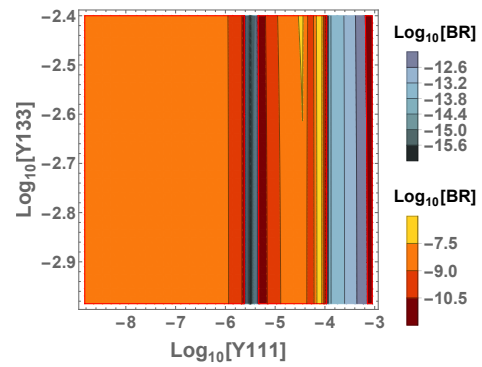
(a) Contourplot with  $\tan \beta = 0.1$ .



(b) Contourplot with  $\tan \beta = 0.9$ .

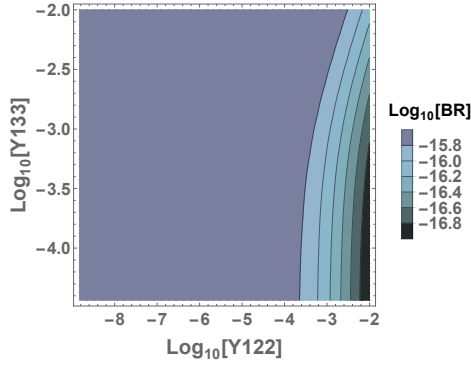


(c) Contourplot with  $\tan \beta = 1.1$ .

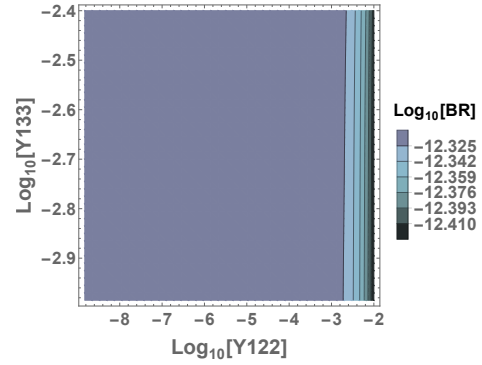


(d) Contourplot with  $\tan \beta = 10$ .

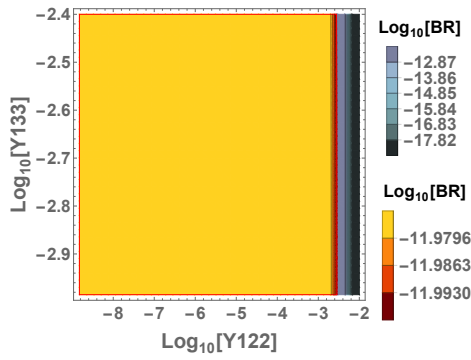
Figure 6.11.. Third solution: In all four plots  $Y_{122} = 10^{-5}$  is a fixed value. Axes and colouring display the same as in figure 6.1. Parts that appear to be independent of  $Y_{133}$  have been magnified.



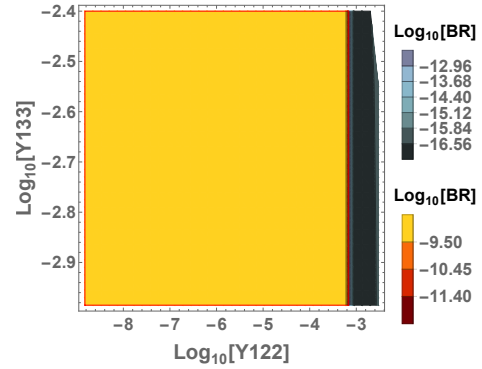
(a) Contourplot with  $\tan \beta = 0.1$ .



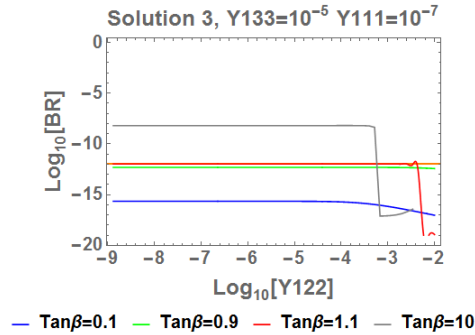
(b) Contourplot with  $\tan \beta = 0.9$ .



(c) Contourplot with  $\tan \beta = 1.1$ .

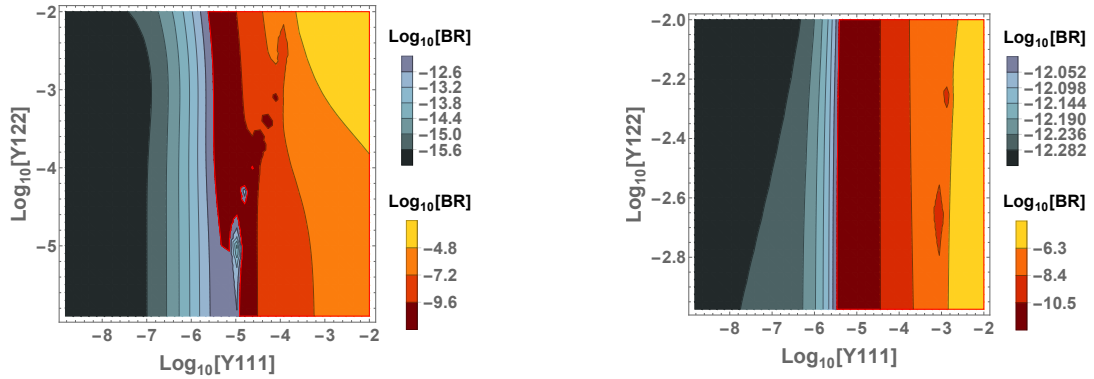


(d) Contourplot with  $\tan \beta = 10$ .



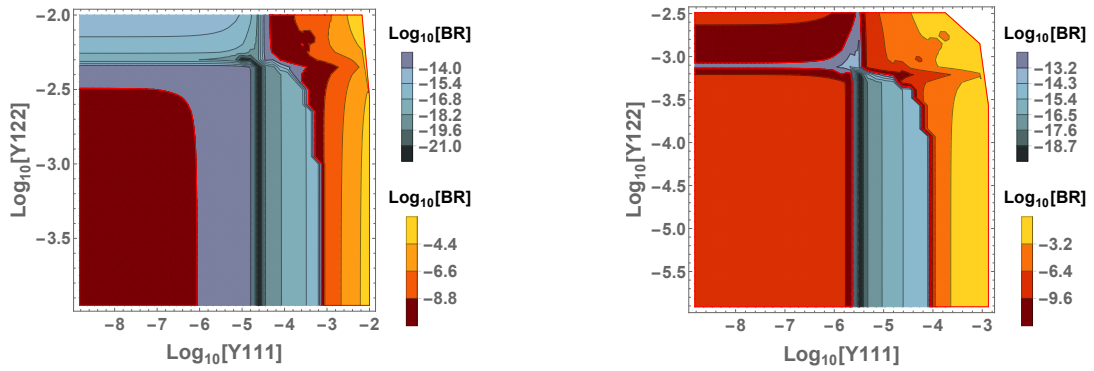
(e) Like before, several values of  $\tan \beta$  were used to compute  $\log_{10} [BR]$  as a function of  $\log_{10} [Y122]$ . The orange horizontal line denotes  $BR = 10^{-12}$ .

Figure 6.12.. Third solution: In all plots  $Y111 = 10^{-7}$  is a fixed value. Axes and colouring are analogous to figure 6.3 .



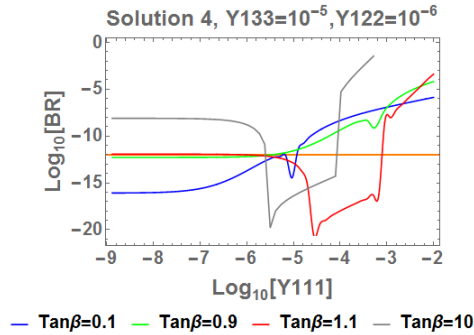
(a) Contourplot with  $\tan\beta = 0.1$ .

(b) Contourplot with  $\tan\beta = 0.9$ .



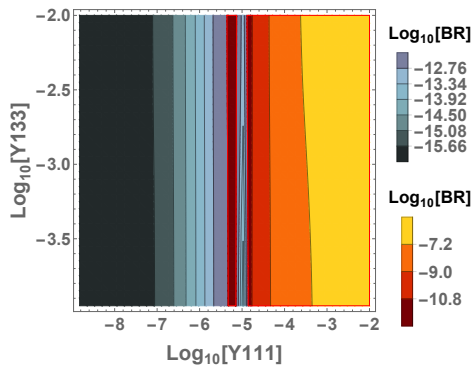
(c) Contourplot with  $\tan\beta = 1.1$ .

(d) Contourplot with  $\tan\beta = 10$ .

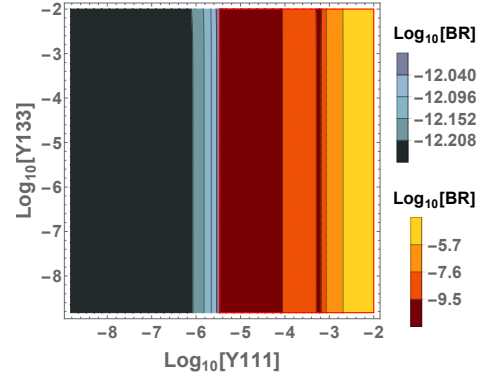


(e) Multiple curves for different values of  $\tan\beta$  at fixed  $Y_{133} = 10^{-5}$  and  $Y_{122} = 10^{-6}$ . The orange line divides the dataset in accepted and rejected regions.

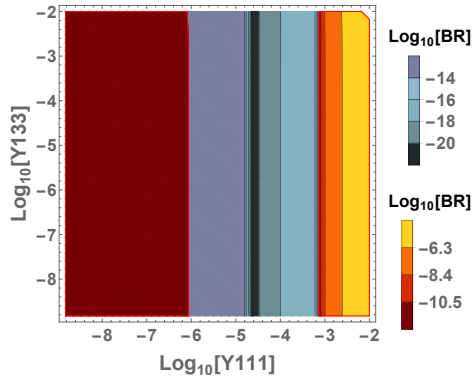
Figure 6.13.. Fourth solution: In all plots  $Y_{133} = 10^{-5}$  is a fixed value. Axes and colouring display the same as in figure 6.1.



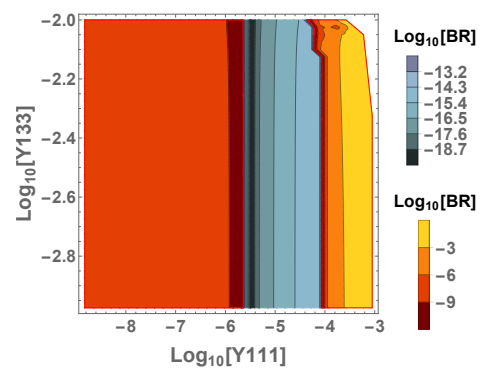
(a) Contourplot with  $\tan \beta = 0.1$ .



(b) Contourplot with  $\tan \beta = 0.9$ .



(c) Contourplot with  $\tan \beta = 1.1$ .

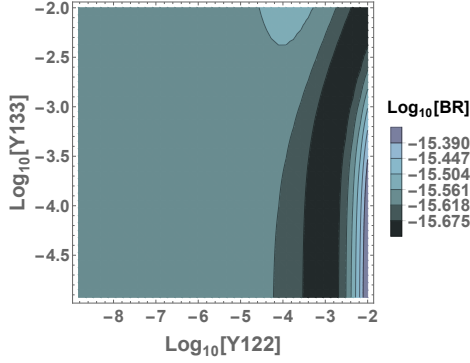


(d) Contourplot with  $\tan \beta = 10$ .

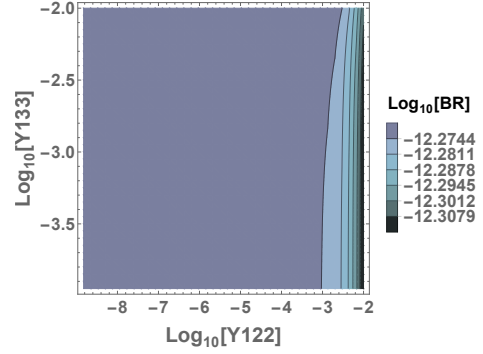
Figure 6.14.. Fourth solution: In all plots  $Y_{122} = 10^{-5}$  is a fixed value. Axes and colouring display the same as in figure 6.3 .

**Fixed Y111**

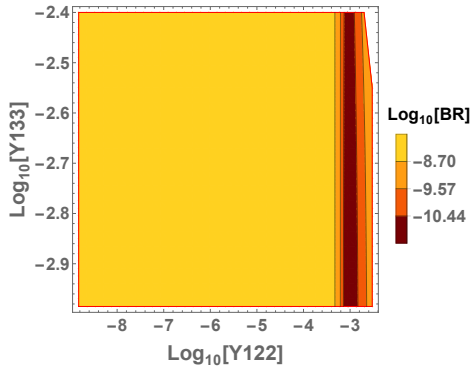
The plots in figure 6.15 show the  $\log_{10} [BR]$  for a fixed value of  $Y_{111} = 10^{-7}$  as a function of  $Y_{122}$  and  $Y_{133}$  just like in figure 6.3.



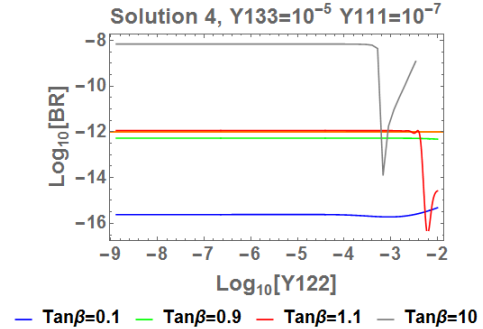
(a) Contourplot with  $\tan \beta = 0.1$ .



(b) Contourplot with  $\tan \beta = 0.9$ .



(c) Contourplot with  $\tan \beta = 10$ .



(d) Like before, several values of  $\tan \beta$  were used to compute  $\log_{10} [BR]$  as a function of  $\log_{10} [Y_{122}]$ . The orange horizontal line denotes  $BR = 10^{-12}$ .

Figure 6.15.. Fourth solution: In all plots  $Y_{111} = 10^{-7}$  is a fixed value. Axes and colouring display the same as in 6.5. Figure 6.15d displays curves with also  $Y_{133} = 10^{-5}$ .

Once more, the branching ratio for the fourth solution of  $Y_R$  turns out to be independent of  $Y_{133}$  for wide ranges of the parameter space. It is also noteworthy that "a bubble" can be found once more in figure 6.13a at  $\log_{10} [Y_{111}] = -4.8$  and  $\log_{10} [Y_{122}] = -4.3$ , with an additional one in its vicinity. Apart from  $BR(Y_{111})$  in the case of  $Table\ 6.0.\beta < 1$ , which once again seems to be monotonously increasing, save for some valleys, no clear rule can be observed. Detailed numbers can be found in the appendix.

## 6.5. $\tan \beta = 1$

Closer attention should be paid to the case of  $\tan \beta = 1$ . With the definitions of the charged lepton masses and the Dirac neutrino masses, the following holds

$$\begin{aligned}
\sqrt{2}m_L &= Y_1 v_1 + Y_2 v_2 \cdot v_1 \\
\sqrt{2}m_D &= Y_2 v_1 + Y_1 v_2 \cdot (-v_2) \\
\Leftrightarrow \sqrt{2}m_L v_1 &= Y_1 v_1^2 + Y_2 v_2 v_1 \\
-\sqrt{2}m_D v_2 &= -Y_1 v_1 v_2 - Y_2 v_2^2 \\
\Rightarrow \sqrt{2}(m_L v_1 - m_D v_2) &= Y_1 (v_1^2 - v_2^2) \\
m_D &= m_L \frac{v_1}{v_2} - Y_1 \frac{(v_1^2 - v_2^2)}{\sqrt{2}v_2}.
\end{aligned} \tag{6.1}$$

Note that for  $\tan \beta = 1$ , with eq. (5.5)  $v_1 = v_2$  and thus

$$m_D = m_L.$$

This implies that  $Y_R$  is independent of  $Y_1$  and  $Y_2$ , which, however, does not necessarily render  $BR$  independent. Because of the mixing between the bidoublet and triplet couplings, according to eq. (4.1) and (4.2), some contributions (for example the ones from the doubly-charged channel) may well be constant, yet the neutral contributions are not. Figure 6.16 displays curves for all four solutions at constant  $Y_{122} = Y_{133} = 10^{-5}$ .

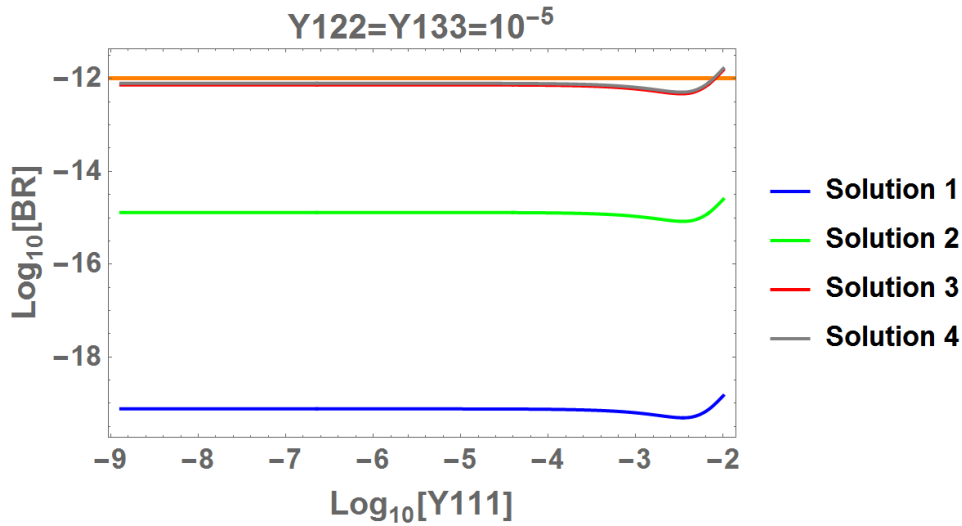


Figure 6.16..  $\log_{10} [BR]$  as a function of  $\log_{10} [Y_{111}]$  with the other Yukawas set to constant values for all four solutions. For most parts of the parameter region, no changes in  $BR$  can be observed.

It turns out that  $BR$  appears to be independent of  $Y_{122}$  and  $Y_{133}$ , which is why just a table containing constant values will be presented.

Thus, for  $\tan \beta = 1$  only the first two solutions prove acceptable within in the whole

## 6. Discussion

	Solution 1	Solution 2	Solution 3	Solution 4
$BR$	$7.56 \cdot 10^{-20}$	$1.30 \cdot 10^{-15}$	$7.35 \cdot 10^{-13}$	$7.95 \cdot 10^{-13}$

Table 6.1.. Branching ratio for all four solutions at  $Y_{111} = 10^{-7}$ ,  $Y_{122} = Y_{133} = 10^{-5}$ .

dataset, whereas the other solutions are very close to the threshold and need to be rejected for  $Y_{111} \approx 10^{-2.5}$ .

## 7. Summary

In the course of this thesis, after a short overview of neutrino physics and the left-right symmetric model, the branching ratio of the muon decay  $\mu^- \rightarrow e^- e^+ e^-$  has been computed in said model. Contrary to the SM, where this decay is forbidden at tree level, there is in fact an allowed tree level amplitude including scalar and pseudoscalar decay channels. After evaluating a phase space integral, the first assumption had to be made, which is  $m_e \rightarrow 0$ . As  $m_e/m_\mu < 0.5\%$ . This limit appears both reasonable and simplifies the calculation drastically, as the integration would otherwise be elliptic and it would definitely go way beyond the scope of a master's thesis in physics. After the phase space integration, integrals along the Mandelstam variables  $\bar{s}$  and  $\bar{t}$  had to be evaluated. Quite surprisingly, the interference between charged and neutral scalars turned out to be exactly zero, once the integral was evaluated, leaving us with the conclusion, that no interference between differently charged decay channels is possible in the given limit. Interference between scalars and pseudoscalars in turn are excluded as the limit of real Yukawa couplings has been set. Thus, a final expression for the  $BR$ , as a function of the bidoublet and triplet Yukawas has been computed.

After this Chapter, the Yukawa couplings for the triplet have been rewritten, using the see-saw formula in order to express them in terms of the bidoublet couplings. Note, that in the course of this calculation, quadratic equations had to be solved leading to eight different solutions for  $Y_R$ . However, as two solutions each are – up to three significant digits – equivalent up to a phase of  $-1$ , these are degenerated. Therefore only four different solutions remain. After expressing the bidoublet VEVs as a combination of the  $W$ -mass  $m_W$  and  $\tan \beta$ , the final expression for the branching ratio was only dependent of  $\tan \beta$  and the  $Y_1$  coupling, which has been assumed to be diagonal. Further assumptions are, that  $Y_L = Y_R$ , a normal neutrino mass hierarchy and as an offset for the neutrino mass scale  $m_1 = m_2/100$ .

After the numeric implementation of the function  $BR$ , several slices have been *cut* for all four solutions through the parameter space. The analysed data range for the Yukawas was  $[10^{-9}, 10^{-2}]$  at  $\tan \beta \in \{0.1, 0.9, 1, 1.1, 10\}$ . Unfortunately, no concise restrictions for the discussed parameters can be obtained from these observations, as they merely represent values of a function of *four* parameters, with two of them each set to a constant value. What could be observed, however, was that  $BR$  tended to be independent of  $Y_{133}$ , for most parts in all of the four solutions. In the discussed plots, the  $BR(Y_{111})$  of solutions 1 and 2 for  $\tan \beta < 1$  appeared to be monotonously increasing and independent of  $Y_{122}$  and  $Y_{133}$ . For  $\tan \beta = 1$  all solutions remained independent of  $Y_{122}$  and  $Y_{133}$  and only the region around  $]10^{-3}, 10^{-2}[$  shows dependence of  $Y_{111}$ . In solutions 3 and 4 at  $\tan \beta < 1$ ,  $BR(Y_{111})$  ( $Y_{122}, Y_{133} = \text{const.}$ ) appears to be monotonously increasing, apart from a few valleys. Note, that the limit of real Yukawas lead to an exclusion of some regions in the parameter space. Nonetheless, these regions were mostly already in the

## 7. Summary

---

regions where  $BR$  was already above the threshold of  $10^{-12}$ . Otherwise, a new function for  $BR$  would have to be implemented, including complex couplings and therefore terms were scalars and pseudoscalars mix. This would not only go beyond the scope of this thesis, but it would fail to provide additional insight, as these regions are small and most of them already excluded.

Of course, these results are not highly reliable and only an indication for the behaviour of  $BR$ . More reliable results can be obtained in a more scrupulous analysis of the parameter space, by analysing all four dimensions parameter space, by an evaluation of  $BR$  with the same increment in every dimension. This way, the regions that prove to be independent of  $Y_{133}$  and  $Y_{122}$  could be localized for instance, and, judging from these results, other tendencies might be proven.

Furthermore, as mentioned before, there are several assumptions being made in the course of these computations. Allowing for a model where  $Y_L \neq Y_R$  and allowing  $Y_1, Y_2$  to have off-diagonal entries would yield more robust information. However, such a procedure would require more time and effort as there would be more parameters needed to compute results.

It would also be helpful to analyse the nature of the four different solutions of the triplet Yukawas. It may be possible to find means to identify, if there were solutions among these turning out to be artefacts without any physical relevance.

If everything proceeds according to schedule, the topic of  $\mu \rightarrow 3e$  will experience lower experimental bounds, as the *The Mu3e Experiment* will start with data taking in 2017, according to their official website [10]. This may provide more insight and reliable results, which may then be used to refine the constraints for the Yukawa couplings in the LRM.

# A. Appendix

## A.1. Model Parameters

$m_{L--}$	$9.24233270 \cdot 10^3$ GeV
$m_{R--}$	$4.25333898 \cdot 10^3$ GeV
$m_{h_1}$	$1.26657427 \cdot 10^2$ GeV
$m_{h_2}$	$4.25132117 \cdot 10^3$ GeV
$m_{h_3}$	$8.07069133 \cdot 10^3$ GeV
$m_{h_4}$	$9.91873826 \cdot 10^3$ GeV
$m_{Ah_1}$	$4.42666964 \cdot 10^3$ GeV
$m_{Ah_2}$	$7.25109486 \cdot 10^3$ GeV
$O$	$\begin{pmatrix} -9.46425275 \cdot 10^{-1} & -3.22903090 \cdot 10^{-1} & 3.57667108 \cdot 10^{-3} & -3.39075847 \cdot 10^{-9} \\ -2.58792992 \cdot 10^{-9} & -2.91542729 \cdot 10^{-9} & 2.11662686 \cdot 10^{-11} & 1 \\ -3.22922841 \cdot 10^{-1} & 9.46360471 \cdot 10^{-1} & -1.10768797 \cdot 10^{-2} & 1.92357792 \cdot 10^{-9} \\ -1.91938567 \cdot 10^{-4} & 1.16384277 \cdot 10^{-2} & 9.99932253 \cdot 10^{-1} & 1.22694316 \cdot 10^{-11} \end{pmatrix}$
$O'$	$\begin{pmatrix} -9.46218815 \cdot 10^{-1} & 3.23407809 \cdot 10^{-1} & 8.79448169 \cdot 10^{-3} & 3.34022321 \cdot 10^{-9} \\ -8.36536934 \cdot 10^{-3} & 2.71691536 \cdot 10^{-3} & -9.99961319 \cdot 10^{-1} & -1.25537675 \cdot 10^{-11} \\ -2.53465532 \cdot 10^{-9} & 2.91124141 \cdot 10^{-9} & 4.16683037 \cdot 10^{-11} & -1 \\ 3.23419193 \cdot 10^{-1} & 9.46255783 \cdot 10^{-1} & -1.34629340 \cdot 10^{-4} & 1.93501723 \cdot 10^{-9} \end{pmatrix}$

Table A.1.. Higgs masses and mixing parameters [8]. Note that the third and fourth column of  $R'$  are required to calculate  $\widetilde{Y}'_i$

## A.2. Readout Parameter Range

	minimum	maximum
$\log_{10} [Y111] \in$	$] - 9.0, -2.2 [$	$] - 9.0, -2.0 [$
$\log_{10} [Y122] \in$	$] - 9.0, -4.2 [$ $\cup ] - 2.6, -2.1 [$	$] - 9.0, -2.0 [$
$\log_{10} [Y133] \in$	$] - 9.0, -2.0 [$	$] - 9.0, -2.0 [$

Table A.2.. for  $\tan \beta < 1$  in the first solution, where all Eigenvalues are positive.

	min part1	min part2	max part1	max part 2
$\log_{10} [Y111] \in$	$] - 9.0, -5.5 [$	$] - 5.6, -5.4 [$	$] - 9.0, -4.4 [$	$] - 5.5, -4.0 [$
$\log_{10} [Y122] \in$	$] - 9.0, -3.1 [$	$] - 3.2, -2.0 [$	$] - 9.0, -2.2 [$	$] - 2.4, -2.0 [$
$\log_{10} [Y133] \in$	$] - 9.0, -2.0 [$	$] - 9.0, -2.0 [$	$] - 9.0, -2.0 [$	$] - 9.0, -2.0 [$

Table A.3.. for  $\tan \beta > 1$  first solution. Minimum/maximum Areas consist of two parts

	min part 1	min part 2	min part 3
$\log_{10} [Y111] \in$	$] - 9.0, -4.9 [$	$< \left(-\frac{0.7}{2.6}\right) \log_{10} [Y122] - 3.7$	$< \left(\frac{0.4}{1.7}\right) \log_{10} [Y133] + 4.0$
$\log_{10} [Y122] \in$	$] - 9.0, -4.6 [$	$] - 4.6, -2.0 [$	$-5.0$
$\log_{10} [Y133] \in$	$] - 9.0, -3.7 [$	$-5.0$	$] - 3.7, -2.0 [$

Table A.4.. Solution 2 min part  $\tan \beta < 1$ . In two columns, one coordinate is approximated by a linear function each.

A.2. Readout Parameter Range

	max 1	max2
$\log_{10} [Y111] \in$	$] - 9.0, -4.1 [$	$< \left(\frac{2.4}{1.1}\right) \log_{10} [Y122] - 3.6 \cdot 10^{-2}$
$\log_{10} [Y122] \in$	$] - 9.0, -3.0 [$	$] - 9.0, -3.0 [$
$\log_{10} [Y133] \in$	$] - 9.0, -2.0 [$	$] - 9.0, -2.0 [$

Table A.5.. maximum for  $\tan \beta < 1$  for Solution 2.

	max 1	max 2
$\log_{10} [Y111] \in$	$] - 9.0, -4.3 [$	$] - 5.5, -2.2 [$
$\log_{10} [Y122] \in$	$] - 9.0, -2.2 [$	$] - 2.2, -2.0 [$
$\log_{10} [Y133] \in$	$] - 9.0, -2.0 [$	$] - 9.0, -2.0 [$

Table A.6.. maximum for  $\tan \beta > 1$  for solution 2

	max part 1	max part 2	max part 3	max part 4
$\log_{10} [Y111] \in$	$] - 5.9, -5.5 [$	$] - 9.0, -5.5 [$	$] - 5.6, -3.3 [$	$< \left(\frac{3}{5}\right) \log_{10} [Y133] - 4.34$
$\log_{10} [Y122] \in$	$] - 9.0, -3.2 [$	$] - 3.4, -3.2 [$	$] - 3.1, -2.5 [$	-5
$\log_{10} [Y133] \in$	-5	-5	-5	$] - 2.6, -2.1 [$
	max part 5	max part 6	max part 7	max part 8
$\log_{10} [Y111] \in$	$] - 5.6, -5.4 [$	$] - 5.9, -5.6 [$	-7	-7
$\log_{10} [Y122] \in$	-5	-5	$] - 3.4, -3.2 [$	$< \left(\frac{2}{3}\right) \log_{10} [Y133] - 1.73$
$\log_{10} [Y133] \in$	$] - 2.1, -2.0 [$	$] - 9.0, -2.6 [$	$] - 9.0, -2.5 [$	$] - 2.5, -2.2 [$

Table A.7.. maximum for  $\tan \beta > 1$  for solution 2

	max part 1	max part 2	max part 3	max part 4
$\log_{10} [Y111] \in$	$] - 9.0, -4.9 [$	$] - 5.2, -4.9 [$ $\cup ] - 9.0, -5.4 [$	$< -\frac{1}{5} < \log_{10} [Y122] + 6.3$	$] - 9.0, -5.2 [$
$\log_{10} [Y122] \in$	$] - 9.0, -5.0 [$	$] - 5.0, -4.6 [$	$] - 4.8, 3.8 [$	-5
$\log_{10} [Y133] \in$	-5	-5	-5	$] - 9.0, -4.0 [$
	max part 5	max part 6	max part 7	max part 8
$\log_{10} [Y111] \in$	$] - 9.0, -5.4 [$	$< -\frac{2}{9} \log_{10} [Y111] - 6.1$	$< -\frac{1}{6} \log_{10} [Y122] - 4.9$	$] - 5.1, -4.9 [$
$\log_{10} [Y122] \in$	-5	-5	$] - 3.8, -2.0 [$	-5
$\log_{10} [Y133] \in$	$] - 9.0, -2.0 [$	$] - 4.0, -3.1 [$	-5	$] - 9.0, -2.0 [$

Table A.8..  $\tan \beta < 1$  max accepted Solution 3.

	max part 9	max part 10
$\log_{10} [Y111] \in$	-7	$] - 9.0, -5.4 [$
$\log_{10} [Y122] \in$	$] - 9.0, -2.0 [$	-5
$\log_{10} [Y133] \in$	$] - 9.0, -2.0 [$	$] - 9.0, -2.0 [$

Table A.9..  $\tan \beta < 1$  max are teil 2 solution3

A. Appendix

	min part 1	min part 2	min part 3
$\log_{10} [Y111]$	$] - 9.0, -5.4 [$	$] - 5.4, -5.3 [$	$-7$
$\log_{10} [Y122]$	$] - 9.0, -3.0 [$	$> 10 \cdot \log_{10} [Y111] - 51$	$] - 9.0, -2.0 [$
$\log_{10} [Y133]$	$-5$	$-5$	$] - 9.0, -2.0 [$

Table A.10.. minimum  $\tan \beta < 1$  Solution3

	max part 1	max part 2	max part 3	max part 4
$\log_{10} [Y111]$	$] - 6.4, -3.8 [$	$] - 3.1, -2.0 [$	$] - 7.0, -6.4 [$	$] - 3.8, -3.6 [$
$\log_{10} [Y122]$	$] - 9.0, -2.6 [$	$] - 9.0, -2.5 [$	$> -3 \log_{10} [Y111] - 28.5$	$> 2 \log_{10} [Y111] + 4.1$
$\log_{10} [Y133]$	$-5$	$-5$	$-5$	$-5$
	max part 5	max part 6	max part 7	max part 8
$\log_{10} [Y111]$	$] - 9.0, -4.4 [$	$] - 4.4, -2.2 [$	$] - 3.6, -3.2 [$	$] - 3.9, -3.5 [$
$\log_{10} [Y122]$	$] - 2.5, -2.0 [$	$> -\log_{10} [Y111] - 0.5$	$> -\frac{5}{4} \log_{10} [Y111] - 7.0$	$] - 3.1, -2.5 [$
$\log_{10} [Y133]$	$-5$	$-5$	$-5$	$-5$
	max part 9			
$\log_{10} [Y111]$	$] - 3.5, -3.3 [$			
$\log_{10} [Y122]$	$] - 9.0, -3.2 [$			
$\log_{10} [Y133]$	$-5$			

Table A.11..  $\tan \beta > 1$  max solution3

	min part 1	min part 2	min part 3	min part 4	min part 5
$\log_{10} [Y111]$	$] - 9.0, -5.5 [$	$] - 5.6, -5.4 [$	$] - 3.9, -3.1 [$	$] - 5.4, -3.9 [$	$] - 4.2, -3.9 [$
$\log_{10} [Y122]$	$] - 3.2, -2.0 [$	$] - 9.0, -3.2 [$	$] - 9.0, -3.2 [$	$] - 3.4, -3.2 [$	$] - 3.9, -3.4 [$
$\log_{10} [Y133]$	$-5$	$-5$	$-5$	$-5$	$-5$
	min part 6	min part 7	min part 8	min part 9	
$\log_{10} [Y111]$	$] - 4.1, -3.9 [$	$] - 6.4, -3.8 [$	$] - 3.4, -3.5 [$	$] - 3.2, -2.0 [$	
$\log_{10} [Y122]$	$> -\log_{10} [Y111] + 8.0$	$-5$	$-5$	$-5$	
$\log_{10} [Y133]$	$-5$	$] - 9.0, -2.0 [$	$] - 9.0, -2.0 [$	$] - 9.0, -2.0 [$	
	min part 10	min part 11	min part 12	min part 13	
$\log_{10} [Y111]$	$] - 6.5, -6.4 [$	$] 10^{-5.6}, 10^{-5.3} [$	$] 10^{-3.9}, 10^{-3.2} [$	$-7$	
$\log_{10} [Y122]$	$-5$	$-5$	$-5$	$] 10^{-2.6}, 10^{-2.0} [$	
$\log_{10} [Y133]$	$> -\frac{1}{12} \log_{10} [Y111] - 6.7$	$] 10^{-9.0}, 10^{-2.0} [$	$] 10^{-9.0}, 10^{-2.0} [$	$] 10^{-9.0}, 10^{-2.0} [$	
	min part 14				
$\log_{10} [Y111]$	$-7$				
$\log_{10} [Y122]$	$] 10^{-3.2}, 10^{-2.0} [$				
$\log_{10} [Y133]$	$] 10^{-9.0}, 10^{-2.0} [$				

Table A.12..  $\tan \beta > 1$  min solution 3

A.2. Readout Parameter Range

	min part 1	min part 2	min part 3	min part 4	min part 5
$\log_{10} [Y111]$	] - 9.0, -5.0 [	] - 9.0, -6.5 [	] - 5.1, -5.0 [	] - 9.0, -5.5 [	] - 5.1, -4.9 [
$\log_{10} [Y122]$	] - 9.0, -5.0 [	] - 5.0, -2.0 [	] - 5.0, -4.6 [	-5	-5
$\log_{10} [Y133]$	-5	-5	-5	] - 9.0, -2.0 [	] - 9.0, -2.0 [
	min part 6		min part 7		
$\log_{10} [Y111]$	-7		] - 9.0, -4.3 [		
$\log_{10} [Y122]$	] - 9.0, -2.0 [		] - 2.5, -2.0 [		
$\log_{10} [Y133]$	] - 9.0, -2.0 [		-5		

Table A.13.. min  $\tan \beta < 1$  Solution4

	min part 1	min part 2
$\log_{10} [Y111]$	] - 9.0, -5.5 [	] - 6.1, -3.2 [
$\log_{10} [Y122]$	] - 9.0, -2.0 [	] - 9.0, -3.1 [
$\log_{10} [Y133]$	-5	-5

Table A.14.. max  $\tan \beta < 1$  Solution4

	min part 1	min part 2	min part 3	min part 4
$\log_{10} [Y111]$	] - 6.1, -3.3 [	] - 6.2, -3.5 [	] - 6.6, -6.2 [	] - 6.2, -6.1 [
$\log_{10} [Y122]$	] - 3.1, -2.7 [	] - 2.7, -2.4 [	$> -\frac{1}{2} \log_{10} [Y111] - 0.8$	$> -4 \log_{10} [Y111] - 27.5$
$\log_{10} [Y133]$	-5	-5	-5	-5
	min part 5		min part 6	
$\log_{10} [Y111]$	] - 4.3, -3.5 [		] - 3.5, -3.3 [	
$\log_{10} [Y122]$	$< -\frac{1}{2} \log_{10} [Y111] - 4.3$		$< -\log_{10} [Y111] - 6.0$	
$\log_{10} [Y133]$	-5		-5	
	min part 7		min part 8	
$\log_{10} [Y111]$	] - 3.3, -3.1 [		] - 6.1, -3.1 [	
$\log_{10} [Y122]$	$< -\log_{10} [Y111] - 6.2$		-5	
$\log_{10} [Y133]$	-5		] - 9.0, -2.0 [	

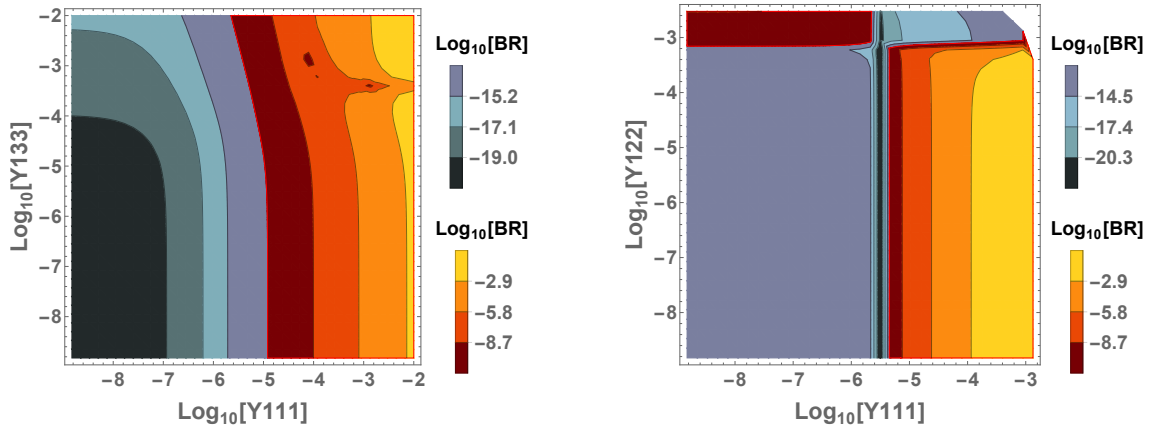
Table A.15.. min  $\tan \beta > 1$  Solution4

### A. Appendix

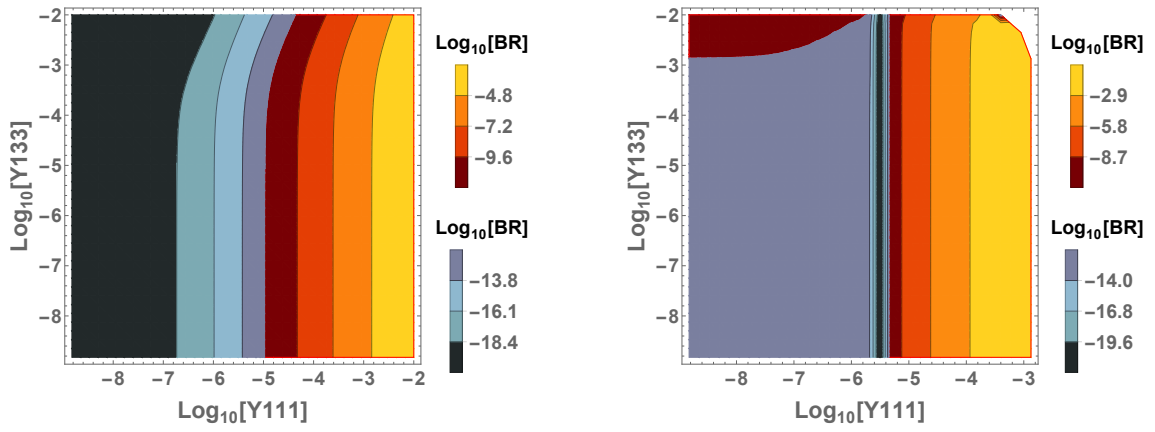
	max part 1	max part 2	max part 3	max part 4	max part 5
$\log_{10} [Y111]$	$] - 5.6, -4.1 [$	$] - 5.6, -4.2 [$	$] - 5.6, -4.5 [$	$] - 5.7, -5.5 [$	$] - 5.5, -5.1 [$
$\log_{10} [Y122]$	$] - 9.0, -4.1 [$	$] - 4.1, -3.6 [$	$] - 3.6, -3.3 [$	$] - 3.3, -2.7 [$	$] - 3.3, -3.1 [$
$\log_{10} [Y133]$	-5	-5	-5	-5	-5
	max part 6	max part 7	max part 8		
$\log_{10} [Y111]$	$] - 5.6, -5.5 [$	$] - 6.3, -5.7 [$	$] - 6.3, -5.5 [$		
$\log_{10} [Y122]$	$] - 2.7, -2.5 [$	$< \log_{10} [Y111] - 3.3$	$< -\frac{1}{4} \log_{10} [Y111] - 7.1$		
$\log_{10} [Y133]$	-5	-5	-5		
	max part 9	max part 10	max part 11	max part 12	
$\log_{10} [Y111]$	$] - 3.6, -3.3 [$	$] - 4.3, -4.1 [$	$] - 5.6, -4.1 [$	$] - 5.6, -4.4 [$	
$\log_{10} [Y122]$	$< -\frac{2}{3} \log_{10} [Y111] - 6.7$	$< -\log_{10} [Y111] - 8.2$	-5	-5	
$\log_{10} [Y133]$	-5	-5	$] - 9.0, -2.0 [$	$] - 9.0, -2.0 [$	
	max part 13	max part 14			
$\log_{10} [Y111]$	$] - 5.6, -4.4 [$	-7	$] - 5.1, -4.4 [$		
$\log_{10} [Y122]$	-5	$] - 3.2, -2.7 [$	$< -\frac{2}{7} \log_{10} [Y111] - 4.6$		
$\log_{10} [Y133]$	$] - 2.1, -2.0 [$	$] - 9.0, -2.0 [$	-5		

Table A.16.. max  $\tan \beta > 1$  Solution4. Also linear approximations have been made here.

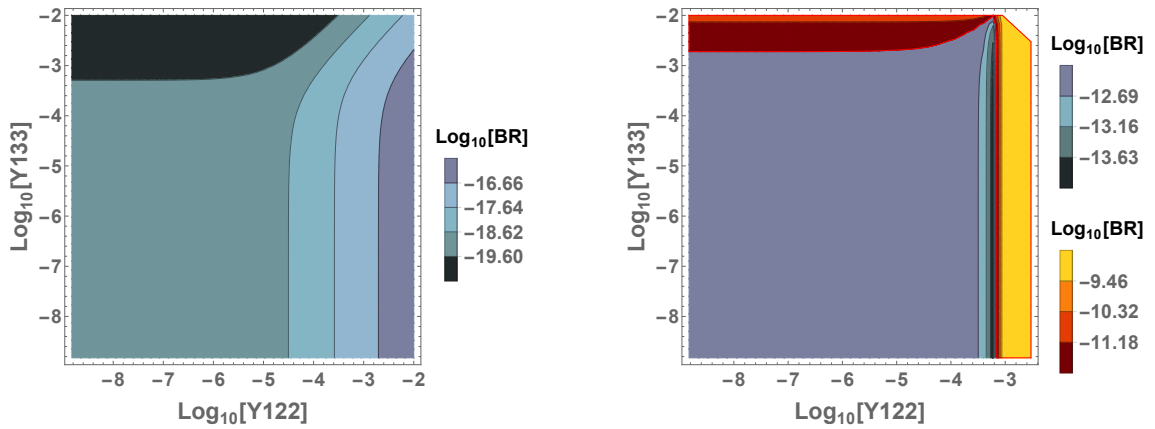
### A.3. Additional Plots



(a) Second solution: Contourplot with  $\tan \beta = 0.5$ . (b) Second solution: Contourplot with  $\tan \beta = 5$ .



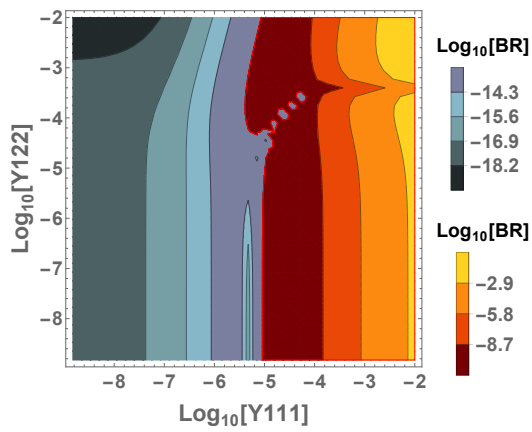
(c) Second solution: Contourplot with  $\tan \beta = 0.5$ . (d) Second solution: Contourplot with  $\tan \beta = 5$ .



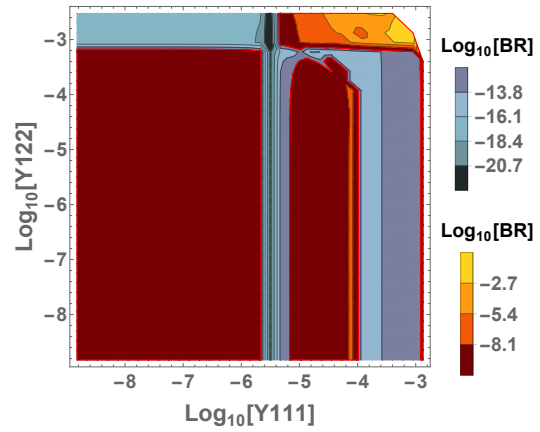
(e) Second solution: Contourplot with  $\tan \beta = 0.5$ . (f) Second solution: Contourplot with  $\tan \beta = 5$ .

Figure A.1.. Contourplots for  $\tan \beta = 0.5$  and 5 in the second solution.

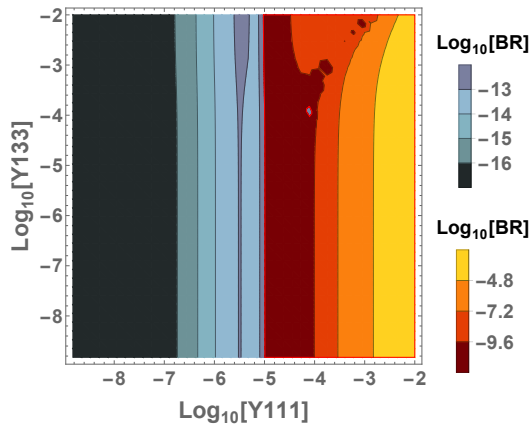
A. Appendix



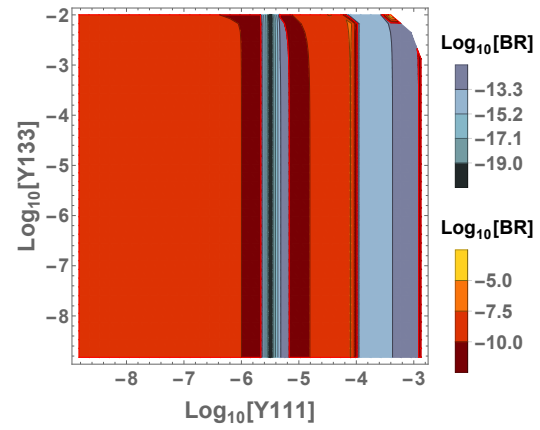
(a) Third solution: Contourplot with  $\tan \beta = 0.5$ .



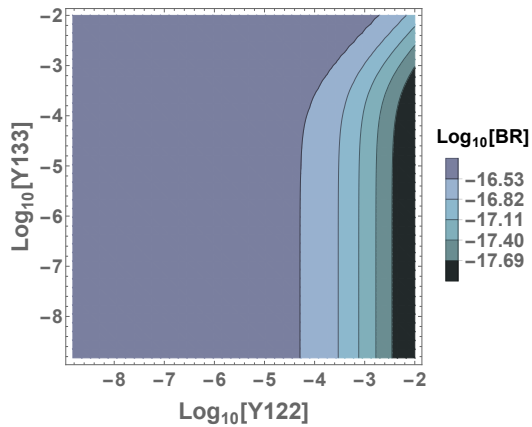
(b) Third solution: Contourplot with  $\tan \beta = 5$ .



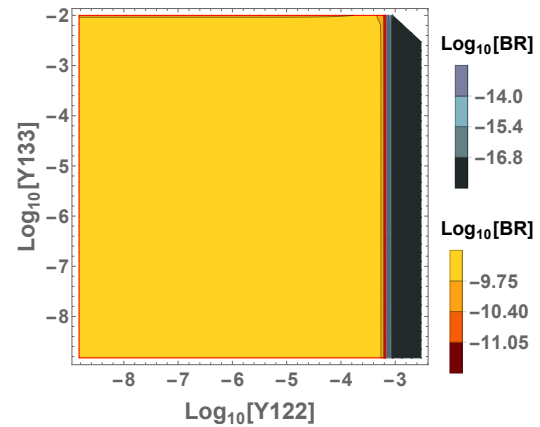
(c) Third solution: Contourplot with  $\tan \beta = 0.5$ .



(d) Third solution: Contourplot with  $\tan \beta = 5$ .

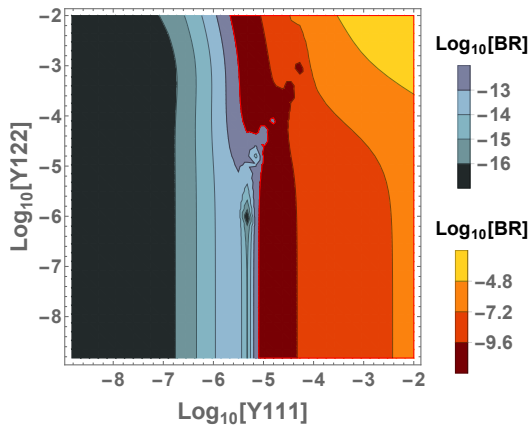


(e) Third solution: Contourplot with  $\tan \beta = 0.5$ .

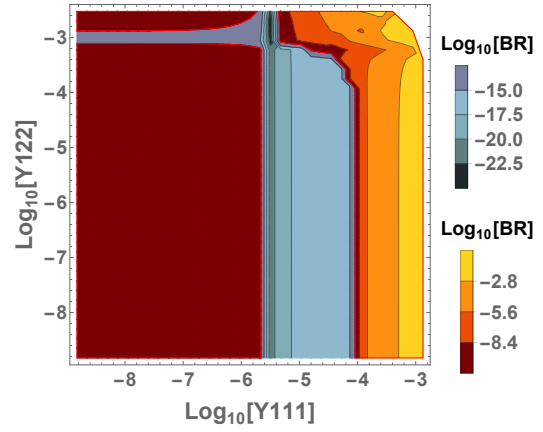


(f) Third solution: Contourplot with  $\tan \beta = 5$ .

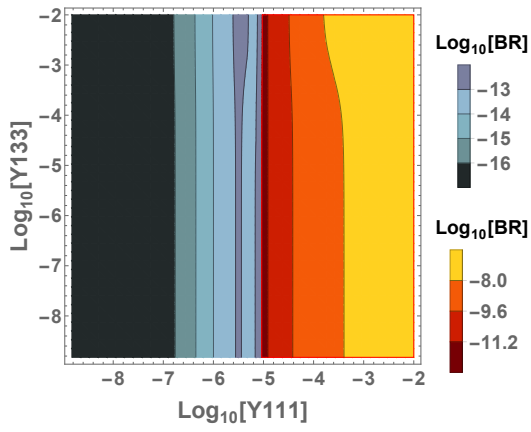
Figure A.2.. Contourplots for  $\tan \beta = 0.5$  and  $5$  in the third solution.



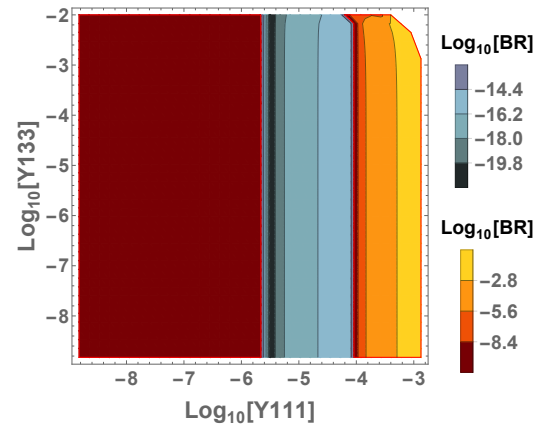
(a) Fourth solution: Contourplot with  $\tan \beta = 0.5$ .



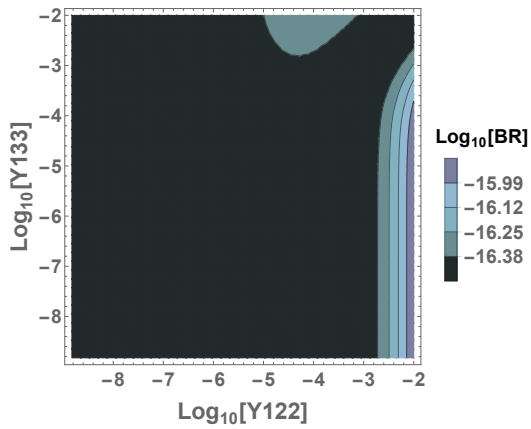
(b) Fourth solution: Contourplot with  $\tan \beta = 5$ .



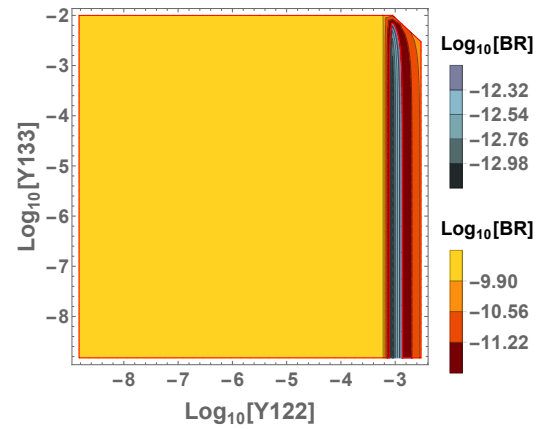
(c) Fourth solution: Contourplot with  $\tan \beta = 0.5$ .



(d) Fourth solution: Contourplot with  $\tan \beta = 5$ .



(e) Fourth solution: Contourplot with  $\tan \beta = 0.5$ .



(f) Fourth solution: Contourplot with  $\tan \beta = 5$ .

Figure A.3.. Contourplots for  $\tan \beta = 0.5$  and  $5$  in the fourth solution.



# Bibliography

- [1] S. Bilenky. *Introduction to the Physics of Massive and Mixed Neutrinos*. 817. Springer-Verlag Berlin Heidelberg, 2010. DOI: [10.1007/978-3-642-14043-3](https://doi.org/10.1007/978-3-642-14043-3).
- [2] M. Blanke et al. “Delta F = 2 observables and  $B \rightarrow X_q \gamma$  decays in the Left-Right Model: Higgs particles striking back”. In: *JHEP* 03 (2012), p. 024. DOI: [10.1007/JHEP03\(2012\)024](https://doi.org/10.1007/JHEP03(2012)024). arXiv: [1111.5014](https://arxiv.org/abs/1111.5014) [hep-ph].
- [3] N. G. Deshpande et al. “Left-right-symmetric electroweak models with triplet Higgs field”. In: *Phys. Rev. D* 44 (3 Aug. 1991), pp. 837–858. DOI: [10.1103/PhysRevD.44.837](https://doi.org/10.1103/PhysRevD.44.837). URL: <http://link.aps.org/doi/10.1103/PhysRevD.44.837>.
- [4] S. L. Glashow, J. Iliopoulos, and L. Maiani. “Weak Interactions with Lepton-Hadron Symmetry”. In: *Phys. Rev. D* 2 (7 Oct. 1970), pp. 1285–1292. DOI: [10.1103/PhysRevD.2.1285](https://doi.org/10.1103/PhysRevD.2.1285). URL: <http://link.aps.org/doi/10.1103/PhysRevD.2.1285>.
- [5] D. Griffiths. *Introduction to elementary particles; 2nd rev. version*. Physics textbook. New York, NY: Wiley, 2008. URL: <https://cds.cern.ch/record/111880>.
- [6] R. Krauber. *The Seesaw Mechanism*. <http://www.quantumfieldtheory.info/TheSeesawMechanism.pdf>. Accessed: 2016-10-02.
- [7] M. Krauß. “Massive Neutrinos in Supersymmetric Models from Higher than  $d = 5$  Effective Operators”. MA thesis. Universität Würzburg, 2010.
- [8] T. Opferkuch M. E. Krauß. private communication.
- [9] K. A. Olive et al. “Review of Particle Physics”. In: *Chin. Phys.* C38 (2014), p. 090001. DOI: [10.1088/1674-1137/38/9/090001](https://doi.org/10.1088/1674-1137/38/9/090001).
- [10] Paul Scherrer Institut. *The Mu3e Experiment*. <https://www.psi.ch/mu3e/introduction>. accessed 2016-10-04.
- [11] M.E. Peskin and D.V. Schroeder. *An Introduction to Quantum Field Theory*. Advanced book classics. Addison-Wesley Publishing Company, 1995. ISBN: 9780201503975. URL: <https://books.google.de/books?id=i35LALN0GosC>.
- [12] W. Porod. private communication.
- [13] W. Porod. *Zerfälle des Gluinos und der Squarks*. Diplomarbeit, Universität Wien. 1993.
- [14] C. Sutton. *Spaceship Neutrino*. Cambridge University Press, 1992. ISBN: 9780521367035. URL: <https://books.google.de/books?id=JB0dejRrmaMC>.
- [15] W. Winter. “Lectures on neutrino phenomenology”. In: *Nuclear Physics B Proceedings Supplements* 203 (June 2010), pp. 45–81. DOI: [10.1016/j.nuclphysbps.2010.08.005](https://doi.org/10.1016/j.nuclphysbps.2010.08.005). arXiv: [1004.4160](https://arxiv.org/abs/1004.4160) [hep-ph].

**Eigenständigkeitserklärung**

Erklärung

Hiermit erkläre ich, dass ich die vorliegende Arbeit selbstständig verfasst und keine anderen als die angegebenen Quellen und Hilfsmittel verwendet und die Arbeit keiner anderen Prüfungsbehörde unter Erlangung eines akademischen Grades vorgelegt habe.

Würzburg, den .....

.....  
(*Unterschrift des Autors*)